# A Grey Wolf Algorithm Based Super Twisted Sliding Mode Controller for an Electric Load Simulator for Testing Actuators of Aircraft Elevator

MOHAMMED ENDRIS YIMER

A Thesis submitted to

The Department of Electrical Power and Control Engineering

School of Electrical Engineering and Computing

Presented in Partial Fulfillment of the Requirement for the Master of Science Degree in Electrical Power and Control Engineering (Control Engineering)

Office of Graduate Studies

Adama Science and Technology University

November, 2022

Adama, Ethiopia

# A Grey Wolf Algorithm Based Super Twisted Sliding Mode Controller for an Electric Load Simulator for Testing Actuators of Aircraft Elevator

MOHAMMED ENDRIS YIMER

Advisor: Dr. Endalew Ayenew

A Thesis Submitted to
The Department of Electrical Power and Control Engineering
School of Electrical Engineering and Computing

Presented in Partial Fulfillment of the Requirement for the Master of Science Degree in Electrical Power and Control Engineering (Control Engineering)

Office of Graduate Studies
Adama Science and Technology University

November, 2022
Adama, Ethiopia

# DECLARATION

I hereby declare that this Master Thesis entitled "A Grey Wolf Algorithm Based Super Twisted Sliding Mode Controller for an Electric Load Simulator for Testing Actuators of Aircraft Elevator" is my original work. That is, it has not been submitted for the award of any academic degree, diploma or certificate in any other university. All sources of materials that are used for this thesis have been duly acknowledged through citation.

| Mohammed Endris Yimer | | |
|---|---|---|
| Name of student | Signature | Date |

# RECOMMENDATION OF ADVISORS

I, the advisors of this thesis, hereby certify that I have read the revised version of the thesis entitled "A Grey Wolf Algorithm Based Super Twisted Sliding Mode Controller for an Electric Load Simulator for Testing Actuators of Aircraft Elevator" prepared under my guidance by Mohammed Endris Yimer submitted in partial of the requirements for the degree of Masters of Science in Electrical Power and Control Engineering. Therefore, I recommend the submission of revised version of the thesis to the department following the applicable procedures.

| ______________________________ | ________________ | ___________________ |
|---|---|---|
| Advisor | Signature | Date |

# APPROVAL PAGE

I, the advisors of the thesis entitled "A Grey Wolf Algorithm Based Super Twisted Sliding Mode Controller for an Electric Load Simulator for Testing Actuators of Aircraft Elevator" and developed by Mohammed Endris Yimer, hereby certify that the recommendations and suggestions made by the board of examiners are appropriately incorporated in to the final version of the thesis.

| Advisor | Signature | Date |
|---|---|---|

We, the undersigned, members of the Board of Examiners of the thesis by Mohammed Endris Yimer have read and evaluated the thesis entitled "A Grey Wolf Algorithm Based Super Twisted Sliding Mode Controller for an Electric Load Simulator for Testing Actuators of Aircraft Elevator" and examined the candidate during open defense. This is, therefore, to certify that the thesis is accepted for partial fulfilment of the requirement of the degree of Master of Science in control engineering.

| | | |
|---|---|---|
| Chairperson | Signature | Date |
| Internal Examiner | Signature | Date |
| External Examiner | Signature | Date |

Finally, approval and acceptance of the thesis is contingent upon submission of its final copy to the Office of Postgraduate Studies (OPGS) through the Department Graduate Council (DGC) and School Graduate committee (SGC).

| | | |
|---|---|---|
| Department Head | Signature | Date |
| School Dean | Signature | Date |
| Office of Postgraduate Studies, Dean | Signature | Date |

# ACKNOWLEDGEMENT

First and foremost, I want to express my gratitude to the Almighty Allah who gave me strength, patience, and courage to complete the thesis successfully. Next my gratitude goes to my advisor Dr. Endalew Ayenew for his invaluable advice, inspiration, motivation, continuous support, and patience during my thesis work. I want to say thank you to Professor Gang Gyoo Jin for his open mind and helping me with giving an idea in order to accomplish my thesis work. Finally, I want to express and send my gratitude and blessing to all of my family and others those assisted me for the accomplishing of thesis.

# TABLE OF CONTENTS

# LIST OF FIGURES

# LIST OF TABLES

# LIST OF ABBRIVATIONS

| | |
|---|---|
| ARTC | Adaptive robust torque control |
| DSP | Digital signal processing |
| ELLS | Electric Linear Load Simulator |
| ELS | Electric Load Simulator |
| EHLS | Electro-Hydraulic Load Simulator |
| GWO | Grey Wolf Optimization |
| GWO-PID | Grey Optimization tuned proportional integral derivative |
| GWO-STSMC | Grey Wolf Optimization tuned super twisted sliding mode control |
| H∞ | H-infinity |
| HIL | Hardware-in-Loop |
| HOSM | High order sliding mode |
| IAE | Integral absolute error |
| ISE | Integral square error |
| ITAE | Integral time absolute error |
| LMI | Linear matrix inequality |
| MATLAB | Matrix Laboratory |
| MIMO | Multiple input multiple output |
| PMSM | Permanent magnet synchronous motor |
| PLS | Pneumatic Load Simulators |
| P | Proportional |
| PI | Proportional integral |
| PID | Proportional integral derivative |
| SMC | Sliding mode control |
| STSMC | Super twisted sliding mode control |
| T-S | Takagi-Sugeno |
| VSC | Variable structure control |
| ZN | Ziegler-Nichols |
| ZN-PID | Ziegler-Nichols proportional integral derivative |

# LIST OF SYMBOLS

| | |
|---|---|
| $\alpha$ | Alpha |
| $\delta_0$ | Aggregate bristle stiffness |
| Z | Average deflection of bristles |
| $\beta$ | Beta |
| $\delta_1$ | Damping coefficient |
| $\delta$ | Delta |
| $\Gamma(t)$ | Disturbance due to the motion of tested actuator |
| $\Psi(t)$ | Disturbance from nonlinear friction torque disturbance |
| G(v) | Function that describes stribeck effect |
| $F_c$ | Kinetic friction force |
| $T_f(t)$ | Nonlinear friction torque disturbance |
| V | Relative velocity the two surface |
| N | Reducer ratio |
| $F_s$ | Static friction force |
| $V_s$ | Stribeck velocity |
| $K_s$ | Torque meter constant |
| $K_u$ | Ultimate gain |
| $P_u$ | Ultimate period |
| $\delta_2$ | Viscous friction |

# ABSTRACT

*The use of an Electric Load Simulator (ELS) is crucial for applying aerodynamic load to an actuation system for testing and qualification of the actuation system. Large extra torque is produced on the load simulator by the movement of the under-tested actuator, friction torque disturbance, and unknown disturbance. The response time and accuracy of the ELS are impacted by this large extra torque, which in turn affects the testing and verification of the actuators of aircraft elevators. By using conventional control techniques, it is challenging to compensate for and suppress the extra torque produced. The mathematical model of ELS is represented using state space and transfer functions. Nonlinear friction torque disturbance is modeled using the LuGre friction model. Super twisted sliding mode controller (STSMC) is used for this system and the parameters of the controller are tuned using the Grey wolf optimization (GWO) algorithm. The GWO tuned PID (GWO-PID) and the Ziegler Nichols tuned PID (ZN-PID) controllers are used for the comparison of the proposed controller. The controller's performance evaluation is done using MATLAB/Simulink. At 1 Hz loading frequency and for reference sine input, GWO-STSMC improved the suppression of the residual torque by 59.31% as compared with ZN-PID and by 22.43% as compared with GWO-PID. The GWO-STSMC also has better performance than GWO-PID and ZN-PID controllers as loading frequency increased. The GWO-STSMC controller also has better performance than ZN-PID and GWO-PID in terms of time domain specification. It has a rise time of 0.08sec, a settling time of 0.78sec, and an overshoot of 4.24%. According to the results, the tracking performance of GWO-STSMC is better than ZN-PID and GWO-PID as the loading frequency increases. GWO-STSMC has a better ability to suppress the large extra torque produced in ELS. For the random reference input, GWO-STSMC outperforms both ZN-PID and GWO-PID controllers.*

**Key words:** Electric Load Simulator, Extra torque, Super Twisted Sliding Mode Controller, Proportional Integral Derivative Controller, Gray-Wolf Optimizer and Ziegler-Nichols.

# CHAPTER ONE

# 1. INTRODUCTION

## 1.1 Background

A variety of different essential tasks are carried out by actuators on aircraft, including adjusting cargo or weapon gates, widening and retracting landing gear, positioning engine inlet guide vanes and thrust reversers, and attempting to adjust flight control surfaces like the elevator, rudder, ailerons, flaps, slats, and spoilers (J. Fu, 2017). During the flight of aircraft, aerodynamic loads affect a flight control system at the control surfaces or fins. The flight control system must respond to these aerodynamic load in order to maintain precise operation. Aircraft actuators must pass testing and verification to ensure that the flight control surface is correctly set and is capable of withstanding imposed aerodynamic loads. The design, testing, and selection procedures for the flight actuators are crucial for a flight to be stable and secure (Ullah et al., 2014). For this task as well as when creating a new product, a load simulator is crucial. It can be used to generate a desired load torque that is proportional to the aerodynamic load and to apply it to the designed new product in order to assess its performance and stability.

Before the invention of motorized load simulators, testing of actuators was performed using mechanical springs or torsion bars. There are a number of drawbacks to conventional testing, such as the inability of the loading devices to adjust to changing loads (L. Wang et al., 2018). In the present era, flight actuators are tested and certified using the load simulator system. The Load Simulators use a loading motor as the Aerodynamic Loading Device. The most popular load simulators, both in practical applications and for academic study, are Electric Load Simulators (ELS). Robotics, aircraft, wind energy, and elevator systems are just a few of the fields that use ELSs (Shamisa & Kiani, 2018).

The flight actuator is connected to the ELS mechanically through a rigid shaft (Qiao et al., 2018). A closed loop system can employ the loading torque generated at the output shaft of the loading motor due to the direct mechanical connection. To enable feedback control, the Torque Sensor measures the loading torque that is produced to the tested actuator. The error is then applied to the torque controller when this feedback signal is compared to the reference loading torque. The motor driver then adjusts the motor torque to achieve the desired torque loading after obtaining an output signal from the control algorithm. Figure 1.1 shows the electric load simulator test bed.

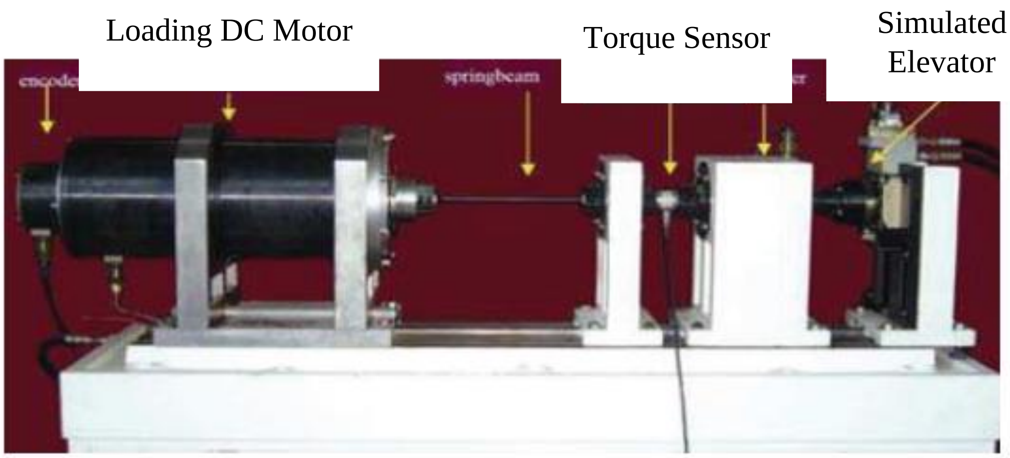


Figure 1.1:- Electric Load Simulator (Li et al., 2018).

The main concern with the load simulator is working out how to get rid of extra torque. The incremental torque, which is caused by the movement of the actuation system, is a large disturbance torque because of the rigid connection between the load simulator and the actuation system (Qiao et al., 2018). In addition to the movement of the actuation system, Friction Force and an Unknown external disturbance also have an impact in addition of extra torque. Because of the effects of this additional torque, testing an actuation system without a torque controller is challenging. Due to nonlinear friction torque disturbance, the system becomes nonlinear. Because of this, it is challenging to control the load torque generated at the shaft of the loading system using traditional control methods such as Proportional Integral Derivative (PID) controllers. Advanced controllers like Sliding Mode Controllers (SMC) are effective in the case of disturbance rejection capability and mitigating the nonlinearity effects.

In this research work, a Grey-Wolf Optimizer based Super twisted sliding mode controller(STSMC) is implemented to control the loading torque of the ELS system. The ELS system's mathematical model is derived in both transfer function and state space. The friction torque disturbance acting on the ELS system is modeled using the LuGre model and then the system is simulated in MATLAB/Simulink.

## 1.2. Statement of the problem

The movement of the under-tested actuator, Friction Torque Disturbance, and Unknown disturbance cause large extraneous torque on an Electrical Load Simulator. This extra torque affects the response speed and precision of the ELS, which in turn affects testing and qualification of actuators of aircraft elevators. The major goal of the controller design in the electric load simulator is attenuation of this large extra torque. But this large extra torque is difficult to compensate for and suppress by conventional control methods. This is due to the fact that the ELS system is highly affected by disturbances and also has a nonlinearity caused by friction torque disturbance. A well-known and accurate friction model as well as the effect of unknown disturbances have not been included in the design or control of the most research works. The loading frequency affect the extra torque produced in ELS. The loading frequency affects the extra torque produced in ELS. In some research papers (Nasim Ullah, 2016), the loading torque controller tracking performance for different loading frequencies is not shown. In addition, in some research papers (Ullah et al., 2014), the loading torque controller tracking performance decreases as the loading frequency increases. This tracking problem, or the occurrence of large extraneous torque, is solved by applying a robust control method. The Super twisted sliding mode controller (STSMC) is one of the robust nonlinear controllers that solve this problem. The parameters of this controller are tuned by the Gray Wolf Optimizer (GWO) to get the best output.

## 1.3 Objective of thesis

### 1.3.1 General objective

The general objective of this research work is to a design GWO based Super twisted sliding mode controller for loading torque tracking of an electric load simulator for the application of testing and qualification of the actuators of an aircraft elevator.

### 1.3.2. Specific objectives

The specific objectives are:

- To derive mathematical model of an Electric Load Simulator system.
- To design the STSMC for torque tracking and PID controllers for comparison.
- To tune the STSMC parameters with GWO algorithms and PID controller parameters with ZN and GWO.

- To evaluate the performance of the developed controller in MATLAB/Simulink by comparing with that of the PID controller.
- To make relevant conclusions and recommendations based on the simulation results.

## 1.4. Scope of the study

The thesis focuses on the mathematical modeling and simulation design of an Electric Load Simulator. Depending on the mathematical mode of the ELS design, STSMC for torque tracking of loading system is designed and simulated in MATLAB/Simulink. STSMC controller parameters are tuned using GWO. The PID controller is designed and its parameters are tuned using Ziegler-Nichols and GWO for comparison.

## 1.5. Limitation of the study

The thesis is restricted to the simulation of the system using MATLAB/Simulink by demonstrating the interactions between the system's parts. This is a result of how challenging it is to acquire the parts required to build a real system. It also accounts for the additional time and money required to build and use the prototype.

## 1.6. Motivation of the study

The design, testing, and selection processes of the flight actuators are essential to ensuring a secure and reliable flight. An efficient flight actuation system can ensure right guidance, hence the importance of testing and qualifying activities cannot be underestimated. One of the reason that leads to airplane crashes is actuation system failure. Real-time actuator testing is essential to mitigating incidents like this. The qualification of the actuators through field testing is a very costly and time-consuming task. Using real flights in the testing process takes more time and money. Using an Electrical Load Simulator is the most effective way to evaluate the stability and effectiveness of rotational and translational actuators in a laboratory environment.

## 1.7. Significance of the study

An essential testing tool in the hardware-in-the-loop simulation of the flight control system in a laboratory environment is an Electrical Load Simulator. Its purpose is to test the effectiveness of the actuator system and simulate the aerodynamic load that the flight actuator will experience during actual operation. It gives information to manufacturers on how well their products are doing before usage and without causing any damage to their property.

## 1.8. Thesis organization

This thesis is organized into six chapters.

**Chapter 1: -** Presents the introduction of the research work, statement of the problems, objectives, significance, scope, and limitations of the research.

**Chapter 2:-** This chapter includes a literature review on an Electric Load Simulator and related work.

**Chapter 3:-** Describes the methods followed in this thesis and the mathematical model of the loading system and loaded system are modeled.

**Chapter 4:-** This chapter presents the control design (STSCM and PID), GWO and Ziegler Nicolas tuning.

**Chapter 5:-** Presents the proposed results and discussions.

**Chapter 6:-** This chapter includes conclusions and recommendations.

# CHAPTER TWO

# 2. LITERATURE REVIEW

## 2.1 Introduction

This chapter mainly discusses the following two parts: The Load Simulator's overview is covered in the first part. The second section includes a review of closely related works, particularly those involving the loading torque control of an Electric Load Simulators with various control strategies and an analysis of their advantages and disadvantages.

## 2.2 Overview of Load Simulator

In a laboratory environment, the Load Simulator simulates the aerodynamic loads imposed on actuators during flight. It investigates if the actuation system's performance satisfies the aircraft's specifications. The airborne actuation system of an aircraft must be tested in a lab environment using a load simulator before it is put through a flying test (Salloum et al., 2016). Because of their significant practical relevance in the testing of aircraft, automotive industry, robotics, and the fault tolerant industry, load simulators have long been a major research topic. A Load Simulator is a crucial piece of equipment in Hardware In Loop (HIL) simulations for aviation control systems that can produce aerodynamic loads on an aircraft's actuation system to evaluate how well they work in real-world conditions. It is a method for anticipating and locating future problems with the mechanical actuator and flight control algorithm. Additionally, it provides a development platform that is substantially more efficient in terms of both time and money (Li et al., 2018).

The mechanical design of the ELS system can be divided into two main sections based on their respective functions: the loading system, which consists of a loading motor and its driver system regarded as a torque servo system, and the actuator under test operated in a position servo mode. Figure 2.1 below illustrates the components of an ELS: a loading motor, a loaded actuator, an angular encoder, and a torque sensor. The structure of ELS is differ based on the application of it.

The tested actuator is directly connected to the loading motor through a rigid shaft. Due to the direct mechanical connection, the loading torque generated at the loading motor's output shaft can be applied to tested actuator. An installed angular encoder is used to record position and speed signals. Applying close-loop torque control is possible due to the torque sensor's (X. Liu et al., 2014).

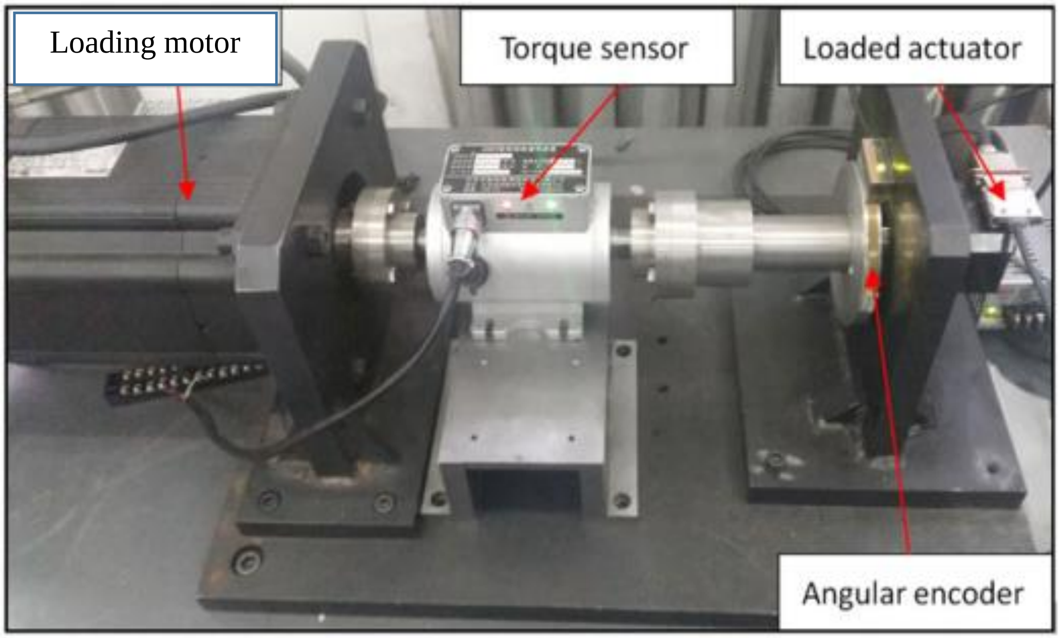


Figure 2.1:- An Electrical Load Simulator (Li et al., 2018).

There are three types of Load Simulators depending on the type of applications and loading requirements. These are;

- Electro-Hydraulic Load Simulators (EHLS)
- Pneumatic Load Simulators(PLS)
- Electrical Load Simulators(ELS)

In flight control applications, Electro-Hydraulic Load Simulators (EHLS) are frequently utilized in hardware-in-the-loop-simulation (HILS) systems that can simulate the aerodynamic load applied to flight actuation systems. The EHLS can simulate loads with massive, quick torque and force and has a high capacity (AKOVA, 2014). Both advantages and drawbacks of EHLS are listed. The EHLS steer and move quickly. The EHLS has a very fast and smooth frequency response since the electro-hydraulic servo valve has a natural frequency that is frequently higher than 100 Hz. At slow speeds, the EHLS operates effectively. The operating speed range for the load simulators is rather broad. However, because of the size and volume, maintenance is expensive. The effects of temperature have a negative influence on performance. Both friction loss and the leakage phenomenon are significant at high and low temperatures, respectively. Leakage of hydraulic fluid or oil is a major drawback. It generates environmental contamination. This may easily start a fire. System failure and system blockage are results of the oil pollution (Tenali, 2007). Another form of hardware-in-loop (HIL) device used to apply medium-range torque/force loads to the actuators under test is the Pneumatic Load Simulator (PLS). The PLS can be used to analyze the deformable fast generated load. The majority of industrial buildings already have compressed air; thus pneumatic systems are commonly employed instead because they are typically more affordable to buy. The PLS use air or any other compressed gas to deliver power. It is challenging to achieve smooth performance, especially at low speeds, due to the high compressibility factor. Similar to this, temperature differences can affect the performance of PLS. PLS require less maintenance than Hydraulic Load Simulators due to their reduced size and volume (Ka'ka et al., 2017). The Electrical Load Simulator is a crucial ground-based hardware tester simulator for flight actuation systems, such as the aircraft's actuator, high-speed elevator system, robotic arm, and aircraft control surfaces. Using ELS, medium and small loads are introduced to the tested actuators. ELS operate better and are less sensitive to temperature variations than hydraulic and pneumatic load simulators. Other benefits include their small size and volume, inexpensive installation and maintenance costs, and great performance. ELS don't pose any risks to the environment (Guo et al., 2006).

Generally, the ELS is coupled directly to the actuation system via rigid shaft connection. The active rotating motion of the actuation system always causes ELS to experience substantial coupling disturbance, which is an inherent disturbance that can sometimes be much larger than the required torque output (Y. Fu et al., 2010).

## 2.3 Related works

Several research papers are reported on the designing appropriate compensation controller to eliminate extra torque which is caused by actuation system, friction torque disturbance and unknown disturbance in an Electric Load Simulator. In this section, the closely related works are reviewed which works on ELS to improve tracking performance of ELS and eliminate surplus torque.

A backstepping sliding mode controller was proposed by the authors in (Zhang et al., 2021), in their research work as a solution to the excess force problem in electric linear load simulators (ELLS). To evaluate the performance of linear steering gear, an Electric Linear Load Simulator (ELLS) is utilized. This technique divides the state of the system into the PMSM mechanical subsystem and the load torque subsystem. Based on the backstepping concept, a terminal sliding mode controller for the PMSM mechanical subsystem has been designed. Traditional PID is used in this paper to compare with the designed controller. After applying the controller designed in this work, the suppression of the residual force at 1Hz and 5Hz is enhanced by 52% and 63%, respectively, in comparison to traditional PID. The limitation of this approach is that it doesn't consider how friction and other disturbances may affect the system.

The torque tracking control of an Electric Load Simulator with active motion disturbance and nonlinearity was proposed in (Li et al., 2018) based on a T-S fuzzy model. The nonlinear motion loading model of an ELS was developed with external disturbances in this paper. First, a nonlinear model of ELS is developed, and then the Takagi-Sugeno fuzzy model is used to represent the friction torque nonlinearity of an Electric Load Simulator. To measure the load system's speed, a state observer is built. A new control strategy named virtual desirable state synthesis is proposed to specify the internal desired states in order to transform the tracking control into a stabilization problem. The $H\infty$ criterion is used to reduce external disturbances, and the well-known quadratic Lyapunov function is used to evaluate the stability of the complete closed-loop model. Meanwhile, by resolving a number of linear matrix inequalities (LMI), the feedback gains and the observer gains are obtained separately. The proposed controller improved performance by 75.6% when compared to the PID approach, according to the results of the comparative experiment. How to further reduce the computational complexity and conservativeness of the proposed method are new challenges that require future study.

For an ELS with a large position coupling disturbance, the authors in (X. Wang et al., 2013) proposed adaptive robust torque control (ARTC). The suggested method aims to reduce the impact of excess torque brought on by the motion of actuation systems, friction torque and uncertain nonlinearities in ELS. The backstepping design via ARTC a lyapunov function is used to construct an ARTC control law for ELS. This paper analyzes and performs an experiment using an aviation actuator. In this study, ARTC control can reduce around 90% of the extraneous torque, but PID control can only eliminate about 83% of it. The limitation with this method is that for modeling friction, a static friction model is used. This model has a simple structure and the parameters in the model are easy to identify, but it cannot accurately describe the friction phenomenon, so the friction compensation based on the static model has limited performance improvement of the system.

In (L. Wang et al., 2016) a speed controller for ELS, to improve the tracking performance and stability of ELS is proposed. In this study, the controller was comprised of terms for load torque compensation, speed reference feedforward, and proportional control. The angle/speed signal and its derivatives from the actuator are used to implement the feedforward compensator. However, various restrictions regarding selecting the feedforward parameters, the higher-order distinguishing of the actuator's angle/speed, and enhancing the control effort reduce the effectiveness of ELS in actual use.

Based on a dynamic load emulation method, the authors in (Lv et al., 2018) proposed the design and modeling of a test bench for dual-motor electric drive tracked vehicles. In the load simulator, the authors employ two motors. While the auxiliary motor serves as a position follower, the primary motor is employed for loading. The position disturbance is roughly minimized, and the initial passive loading is roughly transformed to active loading. The mechanical construction of this scheme needs the synchronous compensation motor loading frequency width to be close to or even more than the load simulator. The volume is big, and the system is difficult to troubleshoot.

Torque control based on torque feedforward and steering gear angle compensation was proposed by the authors in (Gao et al., 2021). The extra force is reduced due to the authors' adoption of the steering gear's angle feedforward compensation and introduction of the torque feedforward compensation approach, however the system exhibits poor characteristics in high-frequency link.

For the purpose of testing and qualifying flight actuators, the authors in (Nasim Ullah, 2016) presented a control approach to reduce surplus torque for the load simulator system. In order to guarantee the high performance torque loop of the aerodynamic loading systems, adaptive fuzzy sliding mode control approaches are presented in this study. A brushless DC motor serves as the tested flight actuator. The loading motor is a permanent magnet synchronous motor (PMSM). The simulation's results demonstrated that the loading motor's output torque matches the reference loading torque. The effectiveness of the suggested torque controller under various loading frequencies is not investigated in this research.

Using dual loop control, in (Jia & Jie, 2018) research was conducted on ELS. This study proposes a twin loop servo loading mechanism. With the use of a two degree of freedom $H\infty$ optimum torque tracking technique, the major goals of this research are to decrease the effect of redundant steering gear torque, further improve the operating frequency band, and increase system durability.

Whether it is active or passive loading, the dual-loop controller suggested in this study will follow the command torque accurately and reduced redundant torque efficiently. The proposed system only considers the motion of loaded actuator as disturbance rather than considering friction and unknown disturbance.

In general, from the above related work, in this section the loading torque/force controls of a load simulator using different controller techniques are reviewed and discussed. Using related works, some research gaps have been identified and defined in this section. Even though a number of research has been done about the torque tracking of ELS system, it is still challenging and it needs additional improvements so as to get the optimal output. This can be achieved by using optimization-based robust control methods.

The research gaps that were observed and solved in this thesis generally are: firstly, many researchers did not consider friction and unknown disturbance, but in real time application, these two are the factors that affect the real system of a plant. Secondly, the effect of loading frequency is not shown in some literature. In some research papers, the tracking performance of the controller decreases as the loading frequency increases. Thirdly, the complexity of the mechanical structure of the designed load simulator and the computational complexity and conservativeness of the proposed method are another gap observed. Finally, in the previous review, the tracking performance of loading torque for an electric load simulator should be improved. These gaps are planned and a statement of the problems are solved in this thesis. In table 2.1 below, the summary of the literature review in short and compact table format is presented to understand the previous related works in what way they passed the approach method, achievement, and gaps in research.

The main contribution of this thesis is the design of a super twisting sliding mode controller for successful tracking of loading torque for an Electric Load Simulator for the application of testing and qualification of the actuator of an aircraft elevator. STSMC parameters for loading torque control are tuned using GWO. PID parameters are tuned using ZN and GWO for comparison. As far as I know, the super twisted sliding mode controller tuned using GWO has never been applied to the torque tracking control of an Electric Load Simulator before.

Table 2.1:- Summery of literature review.

| Authors | Title | Methodology | Achieve | Gap |
|---|---|---|---|---|
| (Zhang et al., 2021) | Backstepping sliding mode control of Electric Linear Load Simulator | Backstepping sliding mode control | Compared with traditional PID the suppression of the residual force at 1Hz and 5Hz is improved by 52% and 63% respectively. | did not consider the effect of friction and unknown disturbances. |
| (Li et al., 2018) | Torque tracking control of ELS with active motion disturbance & nonlinearity based on T-S fuzzy model | H∞ controller | Compared with the PID method, the proposed controller improved performance by 75.6%. | Computational complexity and conservativeness of the proposed method |
| (X. Wang et al., 2013) | Adaptive robust torque control of ELS with strong position coupling disturbance | backstepping design via adaptive robust control Lyapunov function | Eliminate about 90% of extra torque | Inaccurate friction model is used. |
| (L. Wang et al., 2016) | A speed controller for ELS | A proportional control, a speed reference feedforward and a load torque compensation. | Improves the dynamic performance and stability of ELS | Higher-order differentiating of actuator’s angle degrade the performance of ELS in practice. |

| | | | | |
|---|---|---|---|---|
| (Lv et al., 2018) | Design & modeling of a test bench for dual-motor electric drive tracked vehicles based on a dynamic load emulation method | Feedforward compensation | Position disturbance is reduced well. | Mechanical structure is complex, the volume is large, and the system is not easy to debug |
| (Gao et al., 2021) | Torque control based on torque feedforward and steering gear angle compensation. | Angle feedforward compensation. | Excess force is suppressed | Has poor characteristics in the high frequency link. |
| (Nasim Ullah, 2016) | Load simulator system for testing and qualification of flight actuators | Adaptive fuzzy sliding mode control | Good tracking of the reference loading torque. | The effectiveness of the controller at various loading frequencies is not evaluated. |
| (Jia& Jie, 2018) | A research on ELS based on dual loop control. | Two degree of freedom H∞ optimal torque tracking strategy | Reduce the surplus torque effectively | did not consider the effect of friction and unknown disturbances. |

# CHAPTER THREE

# 3. SYSTEM MODELING

## 3.1 Introduction

In this chapter, the material, methodology, the mathematical model of the loading system, redesign of tested system and the modeling of nonlinear friction torque using LuGre model are presented.

## 3.2 Materials

In this research work, software such as MATLAB/2021a, Microsoft Office 2016, and Math Type 6.0 equation editor are used. MATLAB is a computing software which consists of technical toolboxes and Simulink. Microsoft office is used for writing the thesis documentation. Math Type 6.0 is used for writing mathematical formulas and equations in Microsoft office word and PowerPoint presentation tools.

## 3.3 Methodology of the thesis

This thesis' methodology mostly focuses on software algorithms. A flowchart with a complete list of the following tasks will be used to develop the thesis methodology.

The thesis's flow chart is shown in the figure 3.1 below. It starts with a literature review to obtain information on subjects related to an Electric Load Simulator. After analyzing all of the resources, the next step is to complete the mathematical modeling for an electric load simulator, which is the foundation of this thesis. The tested system which is aircraft elevator system is taken from (Tayyeb et al., 2021) and redesigned for this application firstly. The loading torque from the loading system is considered as a disturbance in this system and is taken into account in the mathematical model. The second mathematical model is the loading system model. The motion of the tested actuator is considered as a disturbance in this system and is included in the mathematical model of the loading system. The modeling of the loading system additionally takes into account the interference of nonlinear friction torque disturbance and unknown disturbance like temperature. The influence of an unknown disturbance is very small as compared to the disturbance from the motion of the actuator and nonlinear friction torque disturbance (Chu et al., 2018). As a result, this unknown disturbance is ignored in the mathematical model of the loading system. The torque sensor's dynamics are also modeled. The appropriate controller for this system is chosen, and its parameters are tuned using the GWO algorithm, based on the mathematical model and the characteristics of an electric load simulator. GWO tuned PID (GWO-PID) and Ziegler Nichols tuned PID (ZN-PID) controller is used for the comparison of proposed controller. Furthermore, in tested system which is taken from (Tayyeb et al., 2021), the PID controller is used for the adjustment of the position of the elevator by comparing it with a set point. MATLAB/Simulink will be used as simulation tools.

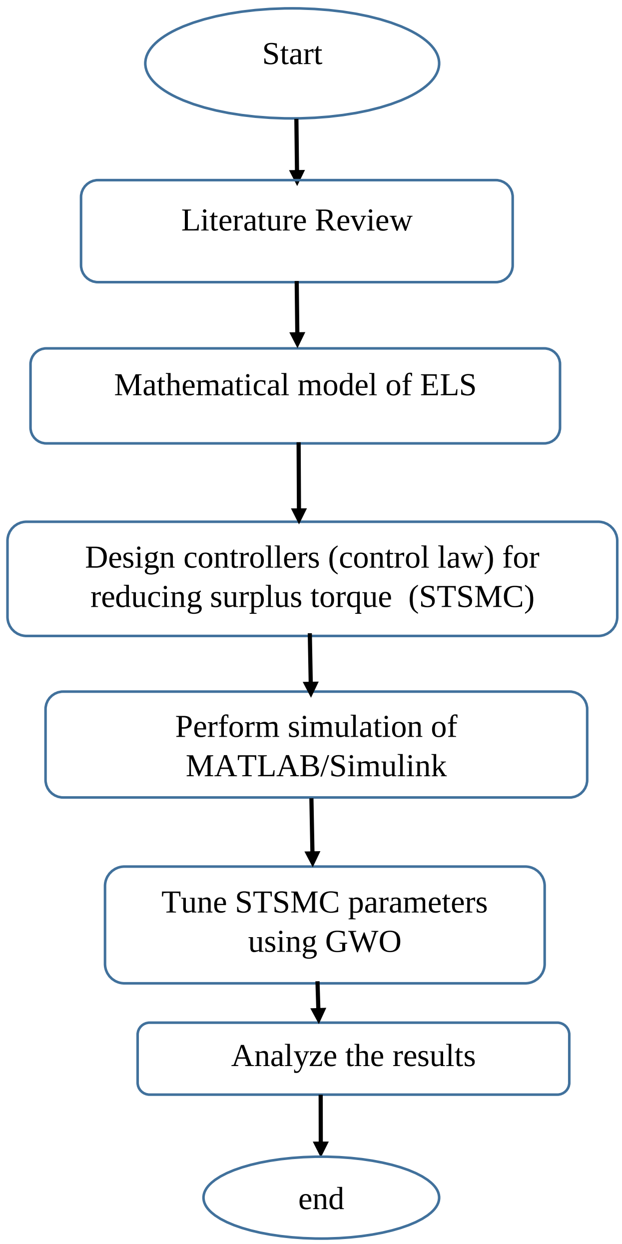


Figure 3.1:- The flow chart of the thesis

## 3.4 Working Principle of an Electric Load Simulator

As shown in Figure 3.2, the ELS is directly connected to the actuation system to simulate the aerodynamic load, with the actuator system on the right and the loading system on the left. The actuation system must follow the required position trajectory in the presence of external disturbances. The loading system, which consists of a DC motor, an angular encoder, and a torque sensor, is indicated on the left. The loading system tracks the desired torque input command, which simulates aerodynamic load acting on the control surface of the actuator system in the flight process. A good ELS system must load an actuator that has undergone testing with the desired torque without adding any extra torque. For the under-tested system to be used as an actuator of aircraft elevator, it must follow the desired position trajectory even in the presence of an external disturbance (i.e., loading torque).

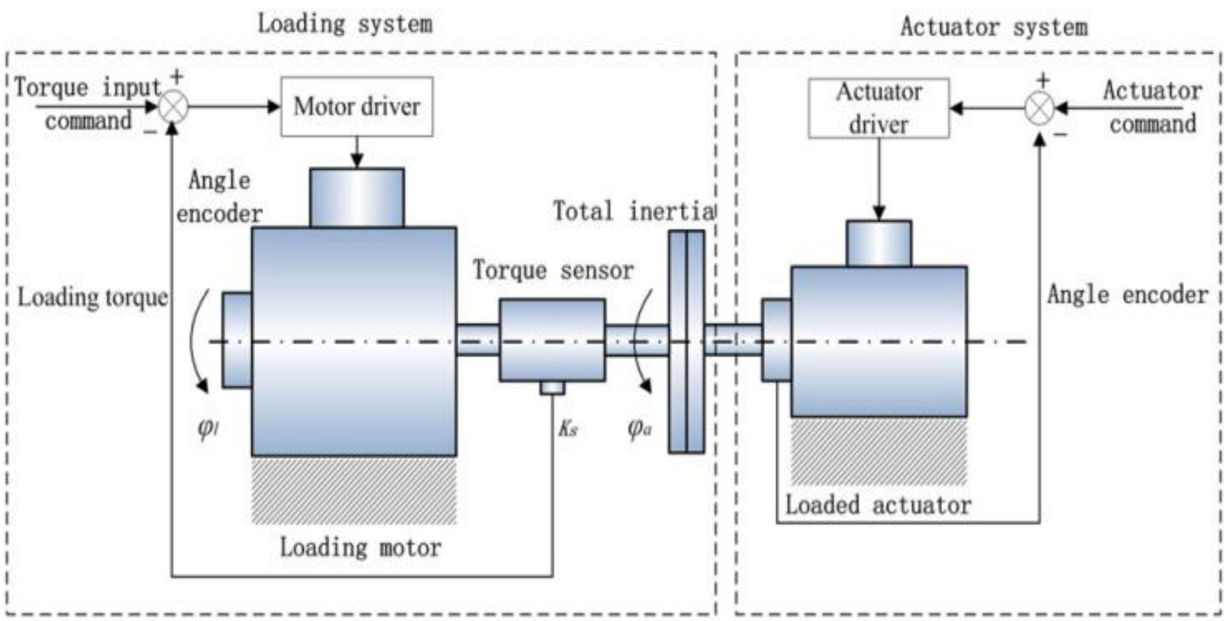


Figure 3.2:- Electrical Load System architecture (Li et al., 2018).

## 3.5 The Proposed Block Diagram for an Electric Load Simulator

As shown in Figure 3.3 below, the proposed system block diagram of an Electrical Load Simulator is a MIMO system.. The system has non-linearity due to the interference of nonlinear friction torque disturbance and there is external disturbance from actuator motion and unknown disturbance. So, to control the system and improve tracking accuracy, it needs a controller. The the proposed ELS control system has two reference inputs. The first reference input is the reference position of the tested system. This system produces disturbances for the loading system. This under-tested system must track position trajectory in the presence of aerodynamic load (i.e., loading torque), which is applied by the loading system. The second input is the reference torque of the loading system. This reference torque is generated from the Load Calculator. The reference position command of the actuator system, Air Speed, Mach Number, and Angle of Attack are the inputs to the Aerodynamic Load Calculator System. The output torque applied to the tested system must track the reference torque. The controller must be designed to track this reference loading torque with an output torque.

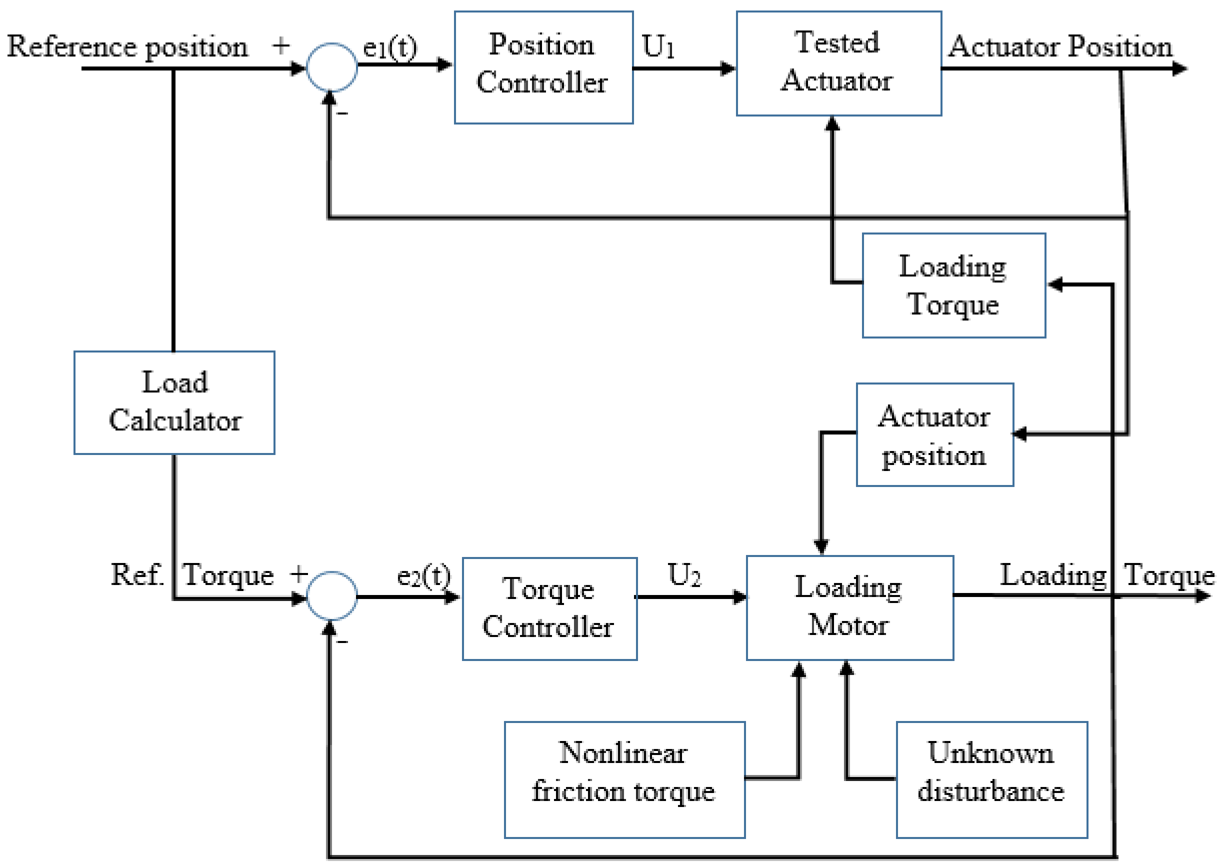


Figure 3.3:- Block diagram of the proposed ELS control system.

Figure 3.3 shows how ELS and tested system are two coupled systems. Output torque can be considered as a disturbance acting on the closed-loop system of the tested system. The motion of the actuator, in contrast, can be regarded as an external disturbance to the torque close loop system since the torque loading system applies the necessary torque to the actuation system when the actuator operates.

## 3.6. Mathematical Modeling of an Electric Load Simulator

As shown in Figure 3.4 below, there are two interrelated subsystems. The first subsystem is the tested system (actuator of aircraft elevator) located on the left side and the second subsystem is loading system which is located on the right side of Figure 3.4.

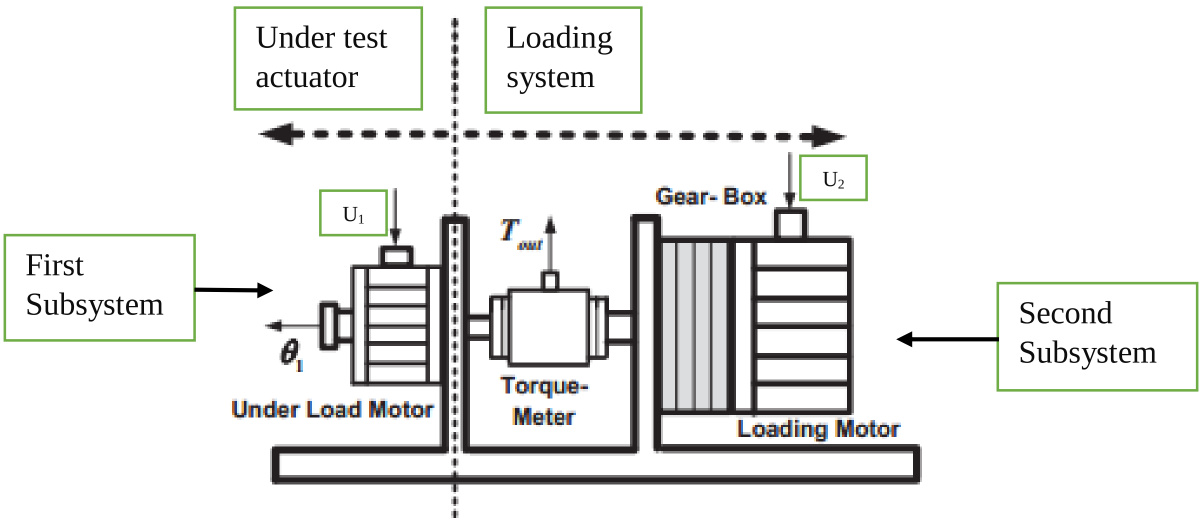


Figure 3.4:- An Electric Load Simulator (Shamisa & Kiani, 2018).

### 3.6.1. First Subsystem Redesign

The first subsystem is PID control based actuator of aircraft elevator and the whole system is taken from the paper in (Tayyeb et al., 2021) and redesigned for this system. DC motor is used as actuator in this system. For simplicity, the DC motor can be used in proportional mode. Then, the electromagnetic torque $T_a$ is directly proportional to the control input $U_a$ of the motor driver, and the relationship can be expressed as:

$$T_a(t) = K_a U_a(t) \tag{3.1}$$

where $K_a$ is the proportionality constant.

The torque balance equation of this DC motor is expressed as:

$$T_a(t) = J_a \frac{d^2\theta_a(t)}{dt^2} + B_a \frac{d\theta_a(t)}{dt} + T_{out}(t) \tag{3.2}$$

where $T_a(t)$ is the motor torque in N.m; $Ja$ is the motor inertia in kg.m$^2$; $\theta_a(t)$ is the rotor angle in rad; $Ba$ is the motor damping constant in N.m/(rad/s); $T_{out}(t)$ is the loading torque in N.m.

The torque balance equation of DC motor is expressed in Laplace transform as:

$$T_a(s) = J_a\theta_a(s)s^2 + B_a\theta_a(s)s + T_{out}(s) \tag{3.3}$$

According to Hooke's law (Li et al.,2018), the mathematical model of the torque sensor is:

$$T_{out}(t) = K_s\left(\frac{\theta_m(t)}{N} - \theta_a(t)\right) \tag{3.4}$$

where $K_s$ is the torque meter constant in N.m/rad; $\theta_a(t)$ is the rotor angle of tested motor in rad; $\theta_m(t)$ is the rotor angle of loading motor in rad; $N$ is the Gearbox ratio.

The angular velocity of the actuator can be expressed as:

$$\omega_a(t) = \frac{d\theta_a(t)}{dt} \tag{3.5}$$

By taking the Laplace transform of Equation (3.1) and substituting into Equation (3.3), load torque becomes:

$$T_{out}(s) = K_a U_a(s) - (J_a s^2 + B_a s)\theta_a(s) \tag{3.6}$$

The position of the tested actuator is expressed in the Laplace transform by substituting Equation (3.4) to Equation (3.6) and solve for $\theta_a(s)$ :

$$\theta_a(s) = \frac{K_a}{J_a s^2 + B_a s - K_s} U_a(s) - \frac{K_s / N}{J_a s^2 + B_a s - K_s}\theta_m(s) \tag{3.7}$$

From Equation (3.7), it is concluding that in the first subsystem, the loading system produce disturbance (aerodynamic load) for tested system. In this regards, actuator of aircraft elevator must have responded well with the presence of this disturbance.

By converting the Laplace transform of Equation (3.7) in to the differential equation, the actuator position can be expressed in second order differential equation as:

$$\begin{aligned} &J_a\ddot{\theta}_a(s) + B_a\dot{\theta}_a(s) - K_s\theta_a(s) = K_a U_a(s) - \frac{K_s}{N}\theta_m(s) \\ &\ddot{\theta}_a(t) = r_1 U_a(t) - r_2\dot{\theta}_a(t) + r_3\theta_a(t) - r_4\theta_m(t) \end{aligned} \tag{3.8}$$

where $r_1 = \frac{K_a}{J_a}$, $r_2 = \frac{B_a}{J_a}$, $r_3 = \frac{K_s}{J_a}$ and $r_4 = \frac{K_s}{NJ_a}$

The system can also represented using state space as follow.

Defining $x_{1t}(t) = \theta_a(t)$ and $x_{2t}(t) = \dot{\theta}_a(t)$ as state variable, $y_t(t) = \theta_a(t)$ as output variable and $U_a(t)$ as control input then the state space model of the first subsystem can represented as:

$$\begin{cases} \dot{x}_{1t}(t) = x_{2t}(t) \\ \dot{x}_{2t}(t) = r_3 x_{1t}(t) - r_2 x_{2t}(t) + r_1 U_a(t) - \Omega \end{cases} \tag{3.9}$$

$$y_t(t) = \theta_a(t) \tag{3.10}$$

where $\Omega = r_4 \theta_m(t)$. Here, $\Omega$ is the disturbance which is aerodynamic load (loading torque).

Table 3.1 contains the parameters of the tested actuator, which are used to complete the mathematical model of the tested system driven in the above equations.

Table 3.1:- Tested Actuator parameters value (Tayyeb et al., 2021).

| **Parameter** | **Symbol** | **Value-Dimension** |
|---|---|---|
| Nominal voltage | $U_a$ | 28V |
| Nominal torque | $T_a$ | 6N.m |
| Nominal speed | $\omega_a$ | 11500RPM |
| Inertia | $J_a$ | 0.04Kg.m$^2$ |
| Damping constant | $B_a$ | 0.244Nm/rad/s |
| Drive constant | $K_a$ | 10 |

For the task of coupling and to measure torque between rotating shaft the torque meter with torque meter constant ($K_s$) of 1000 N.m/rad is used (Sensors, n.d.). In addition, reducer ratio (N) of 35 is used in an Electric Load Simulator for testing and qualification of flight actuator (Nasim Ullah, 2016).

### 3.6.2. Second Subsystem Modeling

The second subsystem is the loading system, which generates loading torque (also known as an aerodynamic load) for the actuation system that is being tested. For the task of generating aerodynamic load, a brushed DC motor is used as the loading motor. It is relatively easy to control the speed of a brushed DC motor. It is not bound by power frequency, may be converted into a high-speed motor, and simply needs voltage regulation to control the common speed. In addition to being reliable, cost-effective, and suitable for difficult operating situations, brushed DC motors also have other benefits. They have a high torque-to-inertia ratio, which is a great advantage. Due to to this, a brushed DC motors are suitable for a variety of tasks, including electrical propulsion, paper machines, cranes, sewing machines, machine testing, and others (Kapoor et al., 2004).

Similar to loaded actuator, the electromagnetic torque generated at loading motor $T_m(t)$ is directly proportional to the control input $U_d(t)$ of the motor driver, and the relationship can be expressed as:

$$T_m(t) = K_d U_d(t) \tag{3.11}$$

where $K_d$ is the proportionality constant.

In consideration of nonlinear friction torque disturbance, the torque balance equation of this DC motor is expressed as:

$$T_m(t) = J_d \frac{d^2\theta_m(t)}{dt^2} + B_d \frac{d\theta_m(t)}{dt} + T_f(t) + T_q(t) \tag{3.12}$$

where $T_m(t)$ is the motor torque in N.m; $J_d$ is the motor inertia in kg.m$^2$; $\theta_m(t)$ is the rotor angle in rad; $B_d$ is the motor damping constant in N.m/(rad/s); $T_q(t)$ is the load torque that is converted to the motor shaft; $T_f(t)$ is the nonlinear friction torque disturbance.

The torque balance equation of this DC motor is expressed in Laplace transform as:

$$T_m(s) = J_d \theta_m(s) s^2 + B_d \theta_m(s) s + T_f(s) + T_q(s) \tag{3.13}$$

The load torque can be expressed as:

$$T_{out}(t) = N T_q(t) \tag{3.14}$$

where $N$ is the reducer ratio.

By taking the Laplace transfer of Equation (3.11), Equation (3.14) and by substituting Equation (3.11) and $T_q(t)$ from Equation (3.14) into Equation (3.13) gives:

$$K_d U_d(s) = J_d \theta_m(s) s^2 + B_d \theta_m(s) s + \frac{T_{out}(s)}{N} + T_f(s) \tag{3.15}$$

$$\frac{T_{out}(s)}{N} = K_d U_d(s) - J_d \theta_m(s) s^2 - B_d \theta_m(s) s - T_f(s) \tag{3.16}$$

The output torque is expressed using Equation (3.17) as follow:

$$T_{out}(s) = NK_d U_d(s) - N(J_d s^2 + B_d s)\theta_m(s) - NT_f(s) \tag{3.17}$$

Substitute $\theta_m(t)$ from Equation (3.4) into Equation (3.17) and solve for output torque gives:

$$T_{out}(s) = \frac{(K_s K_d / N)}{J_d s^2 + B_d s + \dfrac{K_s}{N^2}} U_d(s) - \frac{K_s (J_d s^2 + B_d s)}{J_d s^2 + B_d s + \dfrac{K_s}{N^2}} \theta_a(s) - \frac{K_s / N}{J_d s^2 + B_d s + \dfrac{K_s}{N^2}} T_f(s) \tag{3.18}$$

From Equation (3.18), it is concluded that extra torque is caused by the effect of motion of loaded actuator (i.e. $\theta_1, \dot{\theta}_1, \ddot{\theta}_1$ ) and friction torque. If the input to the loading system is zero, i.e. $U_d = 0$, then Equation (3.18) is reduced to the following simplified relation:

$$T_{out}(s) = T_{extra} = -\frac{K_s (J_d s^2 + B_d s)}{J_d s^2 + B_d s + \dfrac{K_s}{N^2}} \theta_a(s) - \frac{K_s / N}{J_d s^2 + B_d s + \dfrac{K_s}{N^2}} T_f(s) \tag{3.19}$$

According to Equation (3.19), even though the input to the loading system $U_d(s)$ is zero, excess torque is still acting on the system. The main goal of ELS controller design is to reduce these generated surplus torque in order to generate the appropriate torque on the rotating shaft of the tested actuator. The actuator's rotation and friction torque are the main causes of disturbance in the loading system as shown in Equation (3.19).

Converting the Laplace transform of Equation (3.18) to the differential equation gives:

$$J_d \ddot{T}_{out}(t) + B_d \dot{T}_{out}(t) + \frac{K_s}{N^2} T_{out}(t) = \frac{K_s K_d}{N} U_d(t) - K_s J_d \ddot{\theta}_a(t) - B_d \dot{\theta}_a(t) - \frac{K_s}{N} T_f(t) \tag{3.20}$$

From Equation (3.18) the output torque can be expressed in second order differential equation as follow.

$$\ddot{T}_{out}(t) = K_1 U_d(t) - K_2 \dot{T}_{out}(t) - K_3 T_{out}(t) - K_4 \ddot{\theta}_a(t) - K_5 \dot{\theta}_a(t) - K_6 T_f(t) \tag{3.21}$$

where $K_1 = \dfrac{K_s K_d}{N J_d}$, $K_2 = \dfrac{B_d}{J_d}$, $K_3 = \dfrac{K_s}{N^2 J_d}$, $K_4 = K_s$, $K_5 = \dfrac{K_s B_d}{J_d}$ and $K_6 = \dfrac{K_s}{N J_d}$

The system can also be written in the state space form as follow.

Defining $x_1(t) = T_{out}(t)$ and $x_2(t) = \dot{T}_{out}(t)$ as state variable, $y(t) = T_{out}(t)$ as output variable and $U_d(t)$ as control input then the state space model of second subsystem can be expressed as:

$$\begin{cases} \dot{x}_1(t) = x_2(t) \\ \dot{x}_2(t) = -K_3 x_1(t) - K_2 x_2(t) + K_1 U_d(t) - \Gamma - \Psi \end{cases} \tag{3.22}$$

$$y(t) = T_{out}(t) \tag{3.23}$$

where $\Gamma = K_4 \ddot{\theta}_a(t) + K_5 \dot{\theta}_a(t)$ and $\Psi = K_6 T_f(t)$ . Here, $\Gamma$ is disturbance due to the motion of tested actuator and $\Psi$ is treated disturbance from nonlinear friction torque disturbance.

The load calculator is used in proportional mode for convenience. In proportional mode, the output of the load calculator is directly proportional to the reference instruction of the tested system (Shamisa & Kiani, 2018).

Let $\theta_{ref}(t)$ be the reference input of the control system for the system being tested; the load calculator's output $T_c(t)$ would then be:

$$T_c(t) = T_{ref}(t) = C\theta_{ref}(t) \tag{3.24}$$

where *"C"* represents the proportionality constant. The parameter $T_{ref}(t)$ is set as reference command of the loading system.

Table 3.2 contains the parameters of the loading system, which are used to complete the mathematical model of the loading system driven in the above equations.

Table 3.2:- Loading system parameters value (Shamisa & Kiani, 2018).

| **Parameter** | **Symbol** | **Value-Dimension** |
|---|---|---|
| Nominal voltage | $U_d$ | 150V |
| Load calculator constant | C | 2 |
| Nominal torque | $T_d$ | 100N.m |
| Nominal speed | $V_d$ | 1500rad/sec |
| Drive constant | $K_d$ | 20 |
| Inertia | $J_d$ | 0.003503Kg.m$^2$ |
| Damping constant | $B_d$ | 0.413N.m/Krpm |

## 3.7 Nonlinear friction torque modeling

Static friction models and dynamic friction models are the two main types of typical friction models. The most popular Static Friction models are the Coulomb Model, the Stribeck Model, the Karnopp Model, and the Armstrong Model. The Static Friction Model is simple to identify and has a basic structure, but it can't perfectly explain the friction phenomena. As a result, the system's performance can only be slightly improved by friction compensation based on the static model. As a result, several researchers have studied dynamic friction models, primarily the Dahl Model, Elastoplastic Model, LuGre Model, and Leuven Model. These dynamic models can relatively describe the friction phenomenon, but the dynamic model's parameters are complex and difficult to identify (Ruan et al., 2021).

Because it includes many of the observed feature of frictional behavior, the LuGre model has gained popularity (Rogner, 2017). The friction force has a negative derivative with respect to slip velocity at low values of slip velocity. One of the basic behavior of friction that contributes to limit-cycle behavior as well as stick-slip oscillations in frictional systems is this negative slope. In addition, it linearized for tiny motions, the LuGre model behaves like a linear spring/damper pair (Do, 2005).

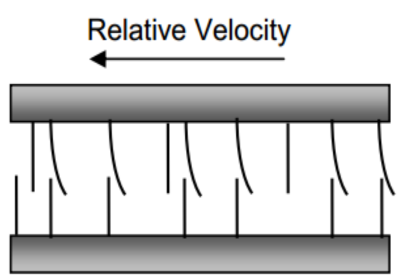


Figure 3.5:- Description of the frictional interface in the LuGre model (Do, 2005).

Figure 3.5 shows a qualitative description of the LuGre model. Two surfaces make contact at different asperities at the microscopic level. Those asperities are represented by bristles, and the bristles behave like springs whenever a relative velocity occurs between the two surfaces. The friction force is occurred by the springs' deflection. If the deflection is high enough, the bristles will randomly slip because of the uneven surfaces. Regarding the unexpected deflection of the bristles, the LuGre model only considers the average deflection. The first-order differential equation models the average deflection of the bristles, Z:

$$\dot{Z} = V - \frac{|V|}{G(V)} Z \tag{3.25}$$

where *V* is the relative velocity between the two surfaces (i.e. loading motor shaft and shaft of tested actuator of aircraft elevator) and *G(V)* is a function that shows the Stribeck effect. The function *G(V)* also expressed as:

$$G(V) = \frac{1}{\delta_0} \left\{ F_c + (F_s - F_c) \exp(-(V / V_s)^2) \right\} \tag{3.26}$$

where $F_c$ is the kinetic friction force, $F_s$ is the static friction force, $\delta_0$ is the aggregate bristle stiffness, and $V_s$ is the Stribeck velocity. Finally, the LuGre friction force is given by the following equation:

$$T_f(V, Z) = \delta_0 Z + \delta_1 \dot{Z} + \delta_2 V \tag{3.27}$$

where $\delta_1$ is a damping coefficient and $\delta_2$ accounts for viscous friction.

The LuGre friction representation in Equation (3.27) is bounded due to the parameters represent $T_f(V, Z)$ like *G(V)* is bounded (i.e., $F_c \leq G(v) \leq F_s$) (Astrom et al., 2009). For this study, the values used for the LuGre parameters are listed in Table 3.3.

Table 3.3:- LuGre Friction Model Parameters (Nasim Ullah, 2016).

| Parameter | Value | Unit |
|---|---|---|
| $\delta_0$ | 260 | Nm/rad |
| $\delta_1$ | 2.5 | Nm-s/rad |
| $\delta_2$ | 0.022 | Nm-s/rad |
| $F_c$ | 2.7 | Nm |
| $F_s$ | 3 | Nm |
| $V_s$ | 0.001 | Rad/sec |

The mathematical model of an Electric Load Simulator is shown in this section using transfer function and in state space approach. Generally, the state space representation of loading system with consideration of nonlinear friction torque disturbance and the redesigned state space representation of tested system are shown below.

Redesigned mathematical model of tested system is:

$$\begin{cases} \dot{x}_{1t}(t) = x_{2t}(t) \\ \dot{x}_{2t}(t) = r_1 U_a(t) + r_3 x_{1t}(t) - r_2 x_{2t}(t) - \Omega \end{cases} \tag{3.28}$$

$$y_t(t) = \theta_a(t) \tag{3.29}$$

where $\Omega = r_4 \theta_m(t)$.

Second subsystem (loading system) mathematical model is:

$$\begin{cases} \dot{x}_1(t) = x_2(t) \\ \dot{x}_2(t) = K_1 U_d(t) - K_3 x_1(t) - K_2 x_2(t) - \Gamma - \Psi \end{cases} \tag{3.30}$$

$$y(t) = T_{out}(t) \tag{3.31}$$

where $\Gamma = K_4 \ddot{\theta}_a(t) + K_5 \dot{\theta}_a(t)$ and $\Psi = K_6 T_f(t)$. Here, $\Gamma$ is disturbance due to the motion of tested actuator and $\Psi$ is treated disturbance from nonlinear friction torque disturbance.

Nonlinear friction torque disturbance is modeled using LuGre friction model and expressed as:

$$T_f(V, Z) = \delta_0 Z + \delta_1 \dot{Z} + \delta_2 V \tag{3.32}$$

where $\dot{Z} = V - \dfrac{|V|}{G(V)} Z$ and $G(V) = \dfrac{1}{\delta_0}\left\{F_c + (F_s - F_c)\exp(-(V/V_s)^2)\right\}$

# CHAPTER FOUR

# 4. CONTROLLER DESIGN

## 4.1 Introduction

Sliding mode control (SMC) is relatively accurate, robust, and simple to tune and implement when compared to other control strategies (Dai et al., 2021). SMC systems are developed to move the system's states onto a certain state space surface called a sliding surface. Once the sliding surface has been arrived, the states there are retained via the SMC. The SMC is therefore a two-part controller. Designing a sliding surface is the initial step. A control law must be chosen as the second task. SMC offers two significant advantages. The first advantage is by selecting a certain sliding function, the system's dynamic characteristics can be altered. Second, some uncertainties have no impact on the closed loop response. This idea is applicable to non-linearity, disturbances, and bounded model parameter uncertainty (Sekhri, 2017). One of the most robust controllers is the Sliding mode controller (SMC), however it has a weakness called chattering. Higher order sliding mode (HOSM) controllers are used to alleviate this issue with regular sliding mode control, and one of these controllers is super twisted sliding mode control (STSMC). The STSMC controller keeps the other characteristics of sliding mode but it avoids the chattering issue (Cucuzzella, n.d.). In this thesis, Grey Wolf Optimization (GWO) is used to tune the STSMC parameters.

In this section, construction of super twisted sliding mode controller (STSMC) for controlling of loading torque in an Electrical Load Simulator and construction of PID for comparison is carried out. The parameters of STSMC are tuned using Grey Wolf Optimization (GWO). The parameters of PID controllers are tuned using Ziegler Nichols (ZN) and Grey Wolf Optimization (GWO).

## 4.2. Sliding Mode Control

SMC is suitable controller for nonlinear systems that are susceptible to external disturbances and model uncertainties (Mancini, 2019).

Consider a system given by:

$$\begin{aligned} \dot{x} &= Ax + Bu + \varphi(t) \\ y &= Cx + Du \end{aligned} \tag{4.1}$$

The variables $y$ and $u$ in this instance stand for the output and input variables, respectively and $\varphi(t)$ represent disturbance and parametric uncertainty.

The control's goal is to make the output variable $y$ follow a specified reference $y_{des}$, this means that the output error variable $e=y-y_{des}$ must go to zero after a reasonable time transient.

As previously mentioned, SMC synthesis is divided into two steps.

a) Sliding surface design

b) Control input design

**a) Sliding surface design**

The tracking error and a number of its variants are used to analyze the sliding surface as follow.

$$s = s(e, \dot{e}, \dots \overset{(k)}{e}) \tag{4.2}$$

The most commonly used type of sliding surfaces are as following.

$$s = \dot{e} + c_0 e \tag{4.3}$$

$$s = \ddot{e} + c_1 \dot{e} + c_0 e \tag{4.4}$$

$$s = e^{(k)} + \sum_{i=0}^{k-1} c_i e^{(i)} \tag{4.5}$$

The number of derivatives in the above equation ($k = r - 1$, where $r$ denotes the input output relative degree). The equation $s = 0$ defines a surface in the error space known as a "sliding surface" from a geometrical perspective. Trajectories of the controlled system are forced onto a sliding surface, where the system behaves as desired (Shtessel et al., n.d.). The sliding surface has the following form.

$$s = (\frac{d}{dt} + c)^k e \tag{4.6}$$

$$\begin{aligned} k &= 1 \quad s = \dot{e} + c_1 e \\ k &= 2 \quad s = \ddot{e} + 2c_1 \dot{e} + c_2{}^2 e \end{aligned} \tag{4.7}$$

whereas $c_1$ and $c_2$ are positive constants.

**b) Control input design**

The second step is to select a control law that drives the variable $s$ to zero in a specific length of time, or a control that steers the system's paths onto the sliding manifold.

There are various SMC:

- Traditional (or first order) SMC and
- High-Order SMC (HOSMC).

### 4.2.1 First Order Sliding Mode Control

The SMC has been developed for a wide range of system types, including MIMO systems, nonlinear and stochastic models, and also models with discrete time and infinite dimensions.

Variable structure control (VSC) accomplishes two objectives by using a high-speed switching control rule. It directing the nonlinear plant's state trajectory onto a particular, user-selected sliding or switching surface in state space. This surface is referred to as the switching surface since a control path has two gains depending on whether the plant's state trajectory is above or below it. Second, for all times, the plant's state trajectory on this surface is retained. VSC refers to a procedure in which the structure of the control system changes from one phase to the next (Rhif et al., 2013).

A variety of control methods are integrated into SMC, a nonlinear control technique, to make sure that trajectories always travel in the direction of a switching state. This means that no single control structure will completely contain the ultimate trajectory (Shtessel et al., n.d.). The main advantage of SMC is its robustness and insensitivity to disturbances and variation in plant parameters, which reduces the need for precise modeling. Another advantage of SMC is the decoupling of the system's overall motion into smaller, independent components. This makes feedback design simpler. Because of its characteristics, SMC has proven to be beneficial in a variety of circumstances.

Across the manifold $s$=0, the control is discontinuous.

$$u = -k \operatorname{sgn}(s) \tag{4.8}$$

whereas

$$u = \begin{cases} -k & s > 0 \\ k & s < 0 \end{cases} \tag{4.9}$$

$k$ is a positive constant.

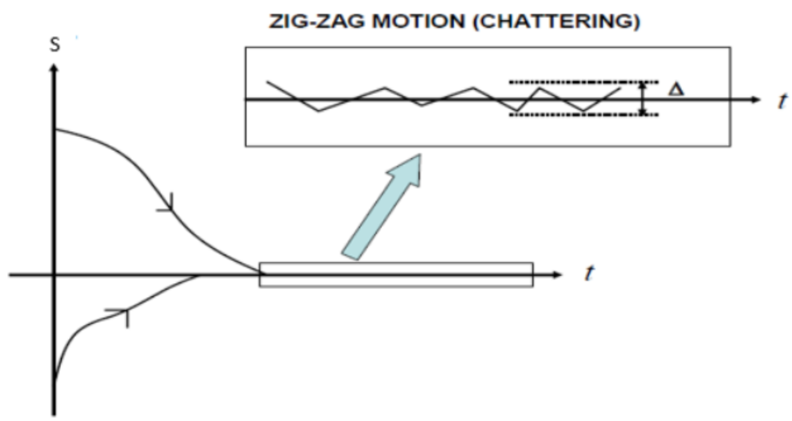


Figure 4.1:- Starting from various initial conditions, a typical evolution of the s variable (Kapoor et al., 2004).

Smoothed implementations of SMC have been suggested to address chattering phenomenon, in which the discontinuous "*sgn*" term is substituted by a continuous smooth approximation function (Rhif et al., 2013).

Two of are as follows.

$$SAT \quad u = -ksat(s,\varepsilon) \equiv -k\frac{s}{|s|+\varepsilon} \quad where \;\; \varepsilon > 0 \quad \varepsilon \approx 0$$

$$TANH \;\; u = -k\tanh(s/\varepsilon) \tag{4.10}$$

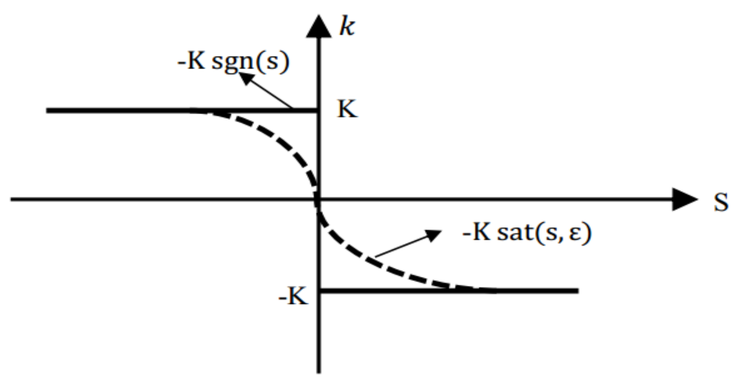


Figure 4.2:- Smooth approximations function (saturation function)(Rhif et al., 2013).

However, in order for this strategy to be effective, there must be no hard uncertainties and the control action to lower them must be set to zero in sliding mode.

### 4.2.2 Second Order Sliding Mode Control

The smooth approximations indicated above can help with some issues, but at the expense of robustness. An efficient substitute that fully resolves the chattering issue while keeping robustness is second order SMC algorithms (Shtessel et al., n.d.). One of the second order SMC algorithm is Super Twisted sliding mode control (STSMC). In order to remove chattering without compromising tracking output, STSMC is a practical substitute for conventional second order SMC for systems of relative degree one (Rhif et al., 2013).

Another method for removing chattering is the high order sliding mode (HOSM) strategy. The primary drawback of this control strategy is that the stability proofs depend on geometrical techniques because it is difficult to demonstrate the Lyapunov function. Due to the fact that the proposed STSMC is based on Lyapunov functions that are quadratic in nature, it is possible to create an explicit relationship between the controller design parameters (Shamisa & Kiani, 2018).

The SMC signal typically consists of two components. One kind of control focuses on sliding surfaces and dynamical systems. It's crucial to use a switching control to keep the system dynamics on the sliding surface (Khan, 2003).

As a result, the sliding surface is expressed as the following:

$$s = qe + \dot{e} \tag{4.11}$$

where $q$ is a sliding constant and $e$ and $\dot{e}$ are the error and error derivative respectively.

The SMC is given by:

$$U = U_{equ} + U_{co} \tag{4.12}$$

where $U_{equ}$ is the equivalent control when system external disturbance and uncertainty are not considered. Its goal is to maintain control over the sliding surface variables. The equivalent control in this equation is obtained by taking into account that the surface's derivative is null i.e., $\dot{s} = 0$. $U_{co}$ is the discrete control, which ensures convergence such that $s\dot{s} \le 0$.

In traditional SMC, switching control is usually adopted as (Becker et al., 2015):

$$U_{co} = -K\,\mathrm{sgn}(s) \tag{4.13}$$

*K* is a positive constant, whereas *sign(s)* is a symbolic function expressed as:

$$\operatorname{sgn}(s)=\begin{cases}-1, & s<0\\ 0, & s=0\\ 1, & s>0\end{cases} \tag{4.14}$$

The effectiveness of conventional SMC is decreased by this switching control's problem, which results in severe chattering in high frequency switches. High order sliding mode control (HOSMC) can eliminate or significantly minimize chattering while maintaining high precision, in addition to offering the same robustness advantages as normal SMC. Super twisted sliding mode control is high order sliding mode control that prevents chattering while preserving the other sliding mode characteristics. It is split into a continuous derivative function and a discontinuous sliding variable function. It is expressed as (J. Liu & Khayati, 2022):

$$\begin{cases}U_{co}=-Y_1\,|s|^{1/2}\operatorname{sgn}(s)+p\\ \\ \dot{p}=-Y_2\operatorname{sgn}(s)\end{cases} \tag{4.15}$$

where $p$ is a continuous function and $Y_1$ and $Y_2$ are constants.

## 4.3 Design STSMC for Loading Torque control of an Electric Load Simulator

The desired system tracking performance is that the load torque $T_{out}(t)$ tracks reference torque $T_{ref}(t)$ as much as possible.

Firstly, design the sliding mode function (sliding surface) as:

$$s=\dot{e}(t)+qe(t) \tag{4.16}$$

where $s$ is sliding surface, $e(t)$ is error and $q$ is positive gain.

Define tracking error for loading torque as:

$$\begin{cases}e(t)=T_{ref}(t)-T_{out}(t)\\ \dot{e}(t)=\dot{T}_{ref}(t)-\dot{T}_{out}(t)\\ \ddot{e}(t)=\ddot{T}_{ref}(t)-\ddot{T}_{out}(t)\end{cases} \tag{4.17}$$

where $e(t)$ is tracking error, $T_{out}(t)$ is load torque and $T_{ref}(t)$ is reference torque.

Therefore, the time derivative of sliding surface can be expressed as:

$$\dot{s}=\ddot{e}(t)+q\dot{e}(t)=(\ddot{T}_{ref}(t)-\ddot{T}_{out}(t))+q(\dot{T}_{ref}(t)-\dot{T}_{out}(t)) \tag{4.18}$$

But,

$$\ddot{T}_{out}(t) = K_1 U_d(t) - K_3 x_1(t) - K_2 x_2(t) - \Gamma - \Psi \tag{4.19}$$

where $\Gamma$ and $\Psi$ are bounded disturbances. $\|\Gamma\| \le g$, this means the disturbance from the motion of tested actuator (i.e., $\theta, \dot{\theta}$) is bounded. The motion of tested actuator is controlled using PID controller. The PID controller is used to control the output position of tested system. As a result, the output position or disturbance of the loading system is bounded due to the PID controller. Nonlinear friction torque is also bounded (i.e., $\|\Psi\| \le m$) (Do, 2005). So that time derivative of sliding surface become:

$$\dot{s} = \ddot{T}_{ref}(t) - K_1 U_d(t) + K_3 x_1(t) + K_2 x_2(t) + \Gamma + \Psi + q(\dot{T}_{ref}(t) - \dot{T}_{out}(t)) \tag{4.20}$$

Take this into account as a Lyapunov candidate function as (Shtessel et al., n.d.):

$$V = \frac{1}{2} s^2 \tag{4.21}$$

$$\dot{V} = s\dot{s} \tag{4.22}$$

$$\dot{V} = s\dot{s} = s(\ddot{T}_{ref}(t) - K_1 U_d(t) + K_3 x_1(t) + K_2 x_2(t) + \Gamma + \Psi + q(\dot{T}_{ref}(t) - x_2(t))) \tag{4.23}$$

Assuming,

$$U_d(t) = \frac{\ddot{T}_{ref}(t) + K_2 x_2(t) + K_3 x_1(t) + q(\dot{T}_{ref}(t) - x_2(t))}{K_1} + v \tag{4.24}$$

Substituting Equation (4.24) to Equation (4.23) we obtain

$$\dot{V} = s(\Gamma + \Psi + v) = s\Gamma + s\Psi + sv \le |s| g + |s| m + sv \tag{4.25}$$

Selecting $v = -L\,\mathrm{sgn}(s)$ where $L>0$ and substituting $v$ into Equation (4.25) gives

$$\dot{V} \le |s| g + |s| m - |s| L = -|s|(L - (g + m)) \tag{4.26}$$

From Equation (4.26), we can conclude that Lyapunov stability requirement is fulfilled. As a result, conventional sliding mode control is design as:

$$U_d(t) = \frac{\ddot{T}_{ref}(t) + K_2 x_2(t) + K_3 x_1(t) + q(\dot{T}_{ref}(t) - x_2(t))}{K_1} - \gamma sgn(s) \qquad or$$

$$U_d(t) = \frac{\ddot{T}_{ref}(t) + K_2 \dot{T}_{out}(t) + K_3 T_{out}(t) + q(\dot{T}_{ref}(t) - \dot{T}_{out}(t))}{K_1} - \gamma sgn(s) \tag{4.27}$$

where $q$ and $\gamma$ are constant.

From Equation (4.27) the designed controller has two parts as:

$$U_{co} = \gamma sgn(s) \qquad and \tag{4.28}$$

$$U_{equ} = \frac{\ddot{T}_{ref}(t) + K_2\dot{T}_{out}(t) + K_3 T_{out}(t) + q(\dot{T}_{ref}(t) - \dot{T}_{out}(t))}{K_1} \tag{4.29}$$

As shown above, the Super twisted sliding mode controller (STSMC) (J. Liu & Khayati, 2022) is given by:

$$\begin{cases} U_{co} = -Y_1 \, | \, s \, |^{1/2} \; \mathrm{sgn}(s) + p \\ \\ \dot{p} = -Y_2 \; \mathrm{sgn}(s) \end{cases} \tag{4.30}$$

where $P$ is continuous function and $Y_1$ and $Y_2$ are constants.

From Equation (4.30) we have

$$U_{co} = -Y_1 \, | \, s \, |^{1/2} \; \mathrm{sgn}(s) - Y_2 \int_0^t \mathrm{sgn}(s) d\tau \tag{4.31}$$

Therefore, from Equation (4.29) and Equation (4.31) the proposed Super twisted sliding mode controller (STSMC) is given by:

$$U_d(t) = U_{equ} + U_{co} \tag{4.32}$$

$$U_d(t) = \frac{\ddot{T}_{ref}(t) + K_2\dot{T}_{out}(t) + K_3 T_{out}(t) + q(\dot{T}_{ref}(t) - \dot{T}_{out}(t))}{K_1} - Y_1 \, | \, s \, |^{\frac{1}{2}} \; \mathrm{sgn}(s) - Y_2 \int_0^t \mathrm{sgn}(s) d\tau \tag{4.33}$$

This designed controller for an Electric Load Simulator (ELS) is evaluated using MATLAB/Simulink. The parameters of Super twisted sliding mode controller (STSMC) $Y_1$, $Y_2$ and $q$ are tuned using Grey Wolf Optimization (GWO). And STSMC are used to control the loading torque. The performance of this controller is compared with that of PID controller. The parameters of PID controller are tuned using the Ziegler-Nichols (ZN) method and Grey Wolf Optimizer (GWO).

Figure 4.3 shows block diagram of loading torque control of an Electrical Load Simulator using STSMC. The parameters of STSMC are tuned using GWO based on cost function.

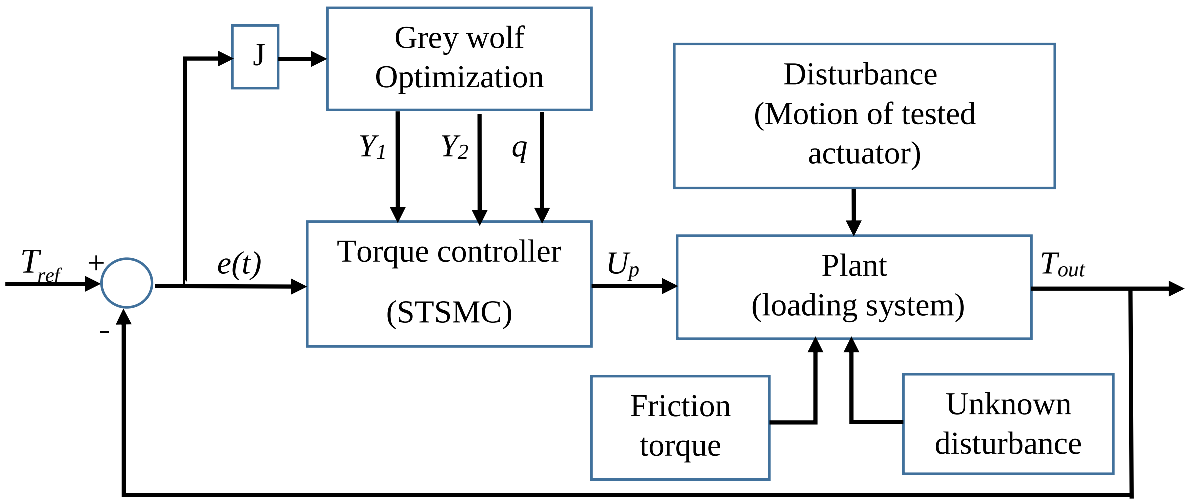


Figure 4.3:- Block diagram of torque control for loading system

## 4.4 PID controller

The PID controller has become the most known controller for use in industrial applications. Designing PID controllers is simple and robust by nature. The final PID algorithm has the following format: where "*U(t)*" denotes for the controller output (Helsinki, 2008).

$$U(t) = K_p e(t) + K_i \int e(t)dt + K_d \frac{d}{dt} e(t) \tag{4.34}$$

whereas $K_p$, $K_i$ and $K_d$ are proportional, integral and derivative gain respectively.

A proportional controller ($K_p$) decreases the rising time and steady-state error but doesn't completely eliminates it. Although an integral control ($K_i$) will eliminate the steady state error, the transient response may be degreded. Derivative control ($K_d$) has the effect of increasing system stability, lowering overshoot, and enhancing transient response. Table 4.1 shows PID controller parametes effect on closed loop system.

Table 4.1:- PID controller parameters effects (Helsinki, 2008).

| Close loop response | Rising time | Overshoot | Settling time | Steady-state error |
|---|---|---|---|---|
| $K_p$ | ↓ | ↑ | Slight change | ↓ |
| $K_i$ | ↓ | ↑ | ↑ | Eliminate |
| $K_d$ | slight change | ↓ | ↓ | Slight change |

## 4.5 Design of the PID Controller for Loading torque control of ELS

PID controller is used for loading torque control of loading system. This PID controller is applied to ELS for the purpose of comparison with STSMC and PID control law is expressed as:

$$\begin{cases} U_p(t) = K_p e(t) + K_i \int e(t)dt + K_d \dfrac{d}{dt} e(t) \\ e(t) = T_{ref}(t) - T_{out}(t) \end{cases} \tag{4.35}$$

whereas $T_{ref}(t)$ is the reference loading torque and $T_{out}(t)$ is the actual measured torque and $K_p$, $K_i$ and $K_d$ are gains of PID controller. These parameters of PID controller are tuned using GWO and ZN to get the desired performance.

In this thesis the tested system is taken from (Tayyeb et al., 2021) and the position of actuator of aircraft elevator is controlled using PID.

## 4.6 Objective Function

Choosing the objective functions that will be used to evaluate each population's fitness is the most crucial stage in adopting any optimization technique. These are just some examples of objective functions (Runyon, 2019).

$$IAE = \int_0^{\tau} | e(t) | \, dt \tag{4.36}$$

$$ISE = \int_0^{\tau} e(t)^2 \, dt \tag{4.37}$$

$$ITAE = \int_0^{\tau} t \, | e(t) | \, dt \tag{4.38}$$

For analyzing the tracking error of the loading system, integral absolute error (*IAE*) in Equation (4.36) is used due to the behavior of less sustained oscillation. This performance index should be minimized to reduce the error.

## 4.7 Grey Wolf Optimization (GWO)

In 2014, Mirjalili et al. introduced the Grey Wolf Optimization (GWO) algorithm (Mirjalili et al., 2014), a search and tuning strategy that mimics the way grey wolves hunt. This technique simulates the social hierarchy and hunting behavior of grey wolf packs in the wild. The grey wolf is a member of a well-organized pack. The four different ranks of wolves in a pack are alpha, beta, delta, and omega. The hierarchy is shown in Figure 4.4 with Alpha (α) as the leader and Beta (β), Delta (δ), and Omega (ω) as the least powerful members. The alpha is the pack's wolf and it has the responsibility of choosing when to sleep, go hunting, and wake up, among other tasks. The remaining wolves in the pack follow the alpha wolf. It is therefore the top-ranking grey wolf in the hierarchy. Beta is the second-highest ranking member in the grey wolf hierarchy. Wolves who assist the alpha with decision-making and other group tasks are known as betas. The beta wolf is the most likely candidate to replace the alpha wolves if one of them dies suddenly or gets too old. The beta wolf is in charge of the lower level wolves but must respect the alpha. The beta gives the alpha feedback from all throughout the pack and approves the alpha's orders. In the wolf hierarchy, omega wolves are the lowest-ranking grey wolf and subordinated by delta wolves, who are on the third rung. Wolves in this group include scouts, sentinels, elders, hunters, and caregivers, to name a few. Scouts are in charge of keeping an eye on the boundaries of the area and alerting the pack to any threats. Sentinels watch over and protect the pack. Wolves who have held the roles of alpha or beta in the past are known as elders. Hunters assist the alphas and betas by killing prey and providing the pack with food. The rank-lowest gray wolf is Omega. The omega is used as a scapegoat (victim-who-is-blamed-for-others' errors or faults). They are the last of the wolves who can eat (Syaifudin, 2015).

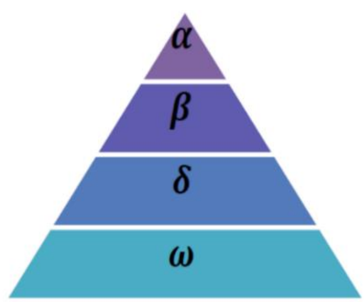


Figure 4.4:- Grey Wolf hierarchy (Syaifudin, 2015)..

The main step of grey wolfs hunting is as shown in Figure 4.5.

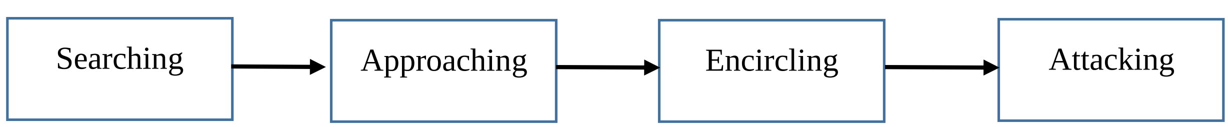


Figure 4.5:- Step of grey wolf hunting (Mirjalili et al., 2014).

Mathematical models of the social hierarchy, as well as models of tracking, surrounding, and attacking prey are illustrated (Verma, 2021).

**a. Social hierarchy**

When developing GWO, alpha ($\alpha$) wolf is the fittest solution is used to mathematically model the social hierarchy of grey wolves. The second and third best solutions are beta ($\beta$) and delta ($\delta$) wolves, respectively. The remaining candidate solutions are omega ($\omega$) wolf. The GWO algorithm's hunting (optimization) is led by $\alpha$, $\beta$ and $\delta$. The omega wolves come after these three wolves.

**b. Encircling prey**

Grey wolves hunt in a circle around their prey. The following are the mathematical models for encircling behavior:

$$\vec{D} = \left|\vec{C}\vec{X}_p(t) - \vec{X}(t)\right| \tag{4.39}$$

$$\vec{X}(t+1) = \vec{X}_p(t) - \vec{A}.\vec{D} \tag{4.40}$$

where *t* is iteration, *X* is position of a grey wolf and $\vec{X}_p$ is position of the prey.

$\vec{A}$ and $\vec{C}$ vectors are determined as:

$$\vec{A} = 2\vec{a}.\vec{r}_1 - \vec{a} \tag{4.41}$$

$$\vec{C} = 2.\vec{r}_2 \tag{4.42}$$

The value of $\vec{a}$ is linearly decrease from 2 to 0. $\vec{r}_1$ and $\vec{r}_2$, are random numbers in between [0,1]. By changing the values of $\vec{A}$ and $\vec{C}$, the top search agents can be reached from different locations based on their current location.

**c. Hunting**

To mathematically represent the hunting behaviors of grey wolves, the first three best answers are saved. The remaining search agents (including the omegas) are then required to adjust their positions in accordance with the status of the top search agents. The following equations are recommended.

$$\vec{D}_\alpha = |\vec{C}_1.\vec{X}_\alpha - \vec{X}|, \quad \vec{D}_\beta = |\vec{C}_2.\vec{X}_\beta - \vec{X}|, \quad \vec{D}_\delta = |\vec{C}_3.\vec{X}_\delta - \vec{X}|, \tag{4.43}$$

$$\vec{X}_1 = \vec{X}_\alpha - \vec{A}_1.(\vec{D}_\alpha), \quad \vec{X}_2 = \vec{X}_\beta - \vec{A}_2.(\vec{D}_\beta), \quad \vec{X}_3 = \vec{X}_\delta - \vec{A}_3.(\vec{D}_\delta), \tag{4.44}$$

$$\vec{X}(t+1) = \frac{\vec{X}_1 + \vec{X}_2 + \vec{X}_3}{3} \tag{4.45}$$

A random population of grey wolves created by GWO is used to start the search. Iteratively, the α, β, and δ wolves determine the likely position of the prey. The separation between the prey and each candidate solution is updated.

**d. Attacking prey**

Grey wolves end the hunting by attacking their prey as it stops moving, as was mentioned previously. The $\vec{a}$ value also reduce the variation range of $\vec{A}$ . When the number of iterations $\vec{A}$ of decrease from 2 to 0, it is said to be at random in the interval [-a, a]. Candidate solutions far away from the prey when $|A| \geq 1$ and approach towards the prey when $|A| < 1$. Finally, $|A| < 1$ force the wolves to assault the prey.

**e. Search for prey**

Grey wolves primarily search based on the α, β, and δ positions. They dispersed to search for prey, then came together to attack it. $\vec{A}$ is utilized to force the search agent to diverge from the prey using random numbers greater or less than 1, in order to mathematically represent divergence. GWO is an optimization algorithm that can function in an uncontrolled manner during the whole optimization process, favoring exploration and avoiding local optima. In contrast to $\vec{A}, \vec{C}$ z is not linearly lowered. GWO requires that C always offer random values at all times, emphasizing exploration/exploitation not only during beginning rounds but also during final iterations.

Stagnation of local optima is a frequent issue, particularly in the final iterations. In these circumstances, this component can be really useful. The GWO algorithm's pseudocode is displayed in Figure 4.6.

```
Initialize population
Initialize a, A, and C
Calculate fitness value. %depending on objective function
Xα=1st fitness
Xβ=2nd best
Xδ=3rd best
While (j < final iterations)
        for each search agent
                Update the position current search agent's by (3.99)
        end
          Update C, a, and A
          Calculate fitness value.  % depending on objective fun. (ITAE)
         Update Xα, Xβ, and Xδ
         j=j+1
end
Return Xα as optimal value of controller (STSMC and PID)
```

Figure 4.6:- The GWO algorithm's pseudocode.

## 4.8 Ziegler Nichols Tuning Method

Two techniques for fine-tuning the parameters of P, PI, and PID controllers were outlined in a 1942 study by Ziegler and Nichols. These two techniques are known as the Ziegler-Nichols closed-loop method and Ziegler-Nichols open-loop method (Haugen, 2010.).

### 4.8.1 Open-loop Tuning Method

The Open-loop method is commonly used to tune PID controllers for plants whose precise dynamics are unknown; however, they can also be utilized with plants whose dynamics are known (MOHAMAD & A, 2012). Based on the transient response behavior of a certain plant, Ziegler and Nichols provided criteria for calculating the values of proportional gain $K_p$, integral time $T_i$, and derivative time $T_d$. Plants that exhibit an S-shaped step response characteristic are tuned using this method (Patel, 2020). The two constants of delay time ($L$) and time constant ($T$) define the S-shaped curve. The S-shaped curve's point of inflection is where a tangent is drawn (Figure 4.7). The time constant, $T$, and the tangent line that intersects with the final value of the step response, $c(t)=K$, are used to calculate the delay time, $L$.

PID controller is also defined as:

$$U = K_p(1 + \frac{1}{T_i s} + T_d s) \quad (4.46)$$

The real usefulness of ZN tuning method is seen when the plant dynamics are unknown (Copeland, 2008). ZN tuning rules' main benefit is that they offer a starting point for determining the parameter values. After obtaining these parameter values ($K_p$, $T_i$, and $T_d$), we can always modify them to further fine-tune the plant's closed-loop reaction and get an acceptable transient response. When tuning using the ZN technique, 25% overshoot is typically attained (Patel, 2020). Ziegler and Nichols recommended setting the parameters Kp, Ti, and Td values in accordance with Table 4.2.

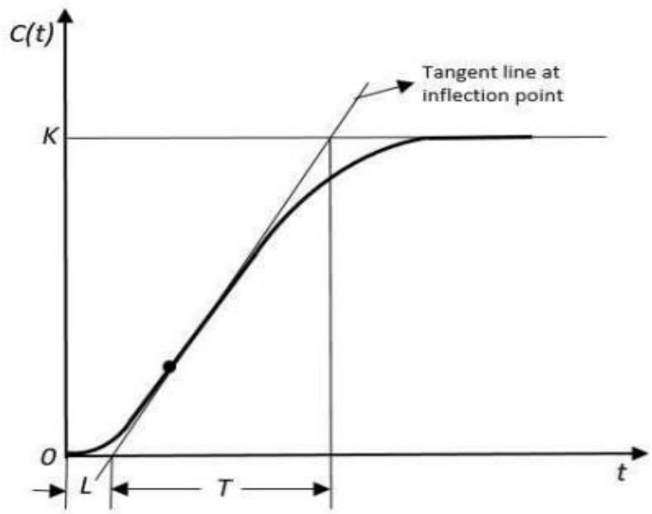


Figure 4.7:- S-shaped step response of a plant (Patel, 2020).

Table 4.2:- Parameter calculation for ZN open_loop tuning method (Patel, 2020).

| **Controllers** | **Parameters** | | |
|---|---|---|---|
| | $K_p$ | $T_i$ | $T_d$ |
| P | $\frac{T}{KL}$ | - | - |
| PI | $\frac{0.9T}{KL}$ | $3.3L$ | - |
| PID | $\frac{1.2T}{KL}$ | $2L$ | $0.5L$ |

### 4.8.2 Ziegler Nichols Close-loop Tuning Method

This method is Called the ultimate cycling method. It is based on experiments executed on a feedback loop of a real system or on simulation if the model is known (Smuts, 2011). The tuning procedure for this method is as follows:

**Step 1**: Turn the PID controller into a P controller by setting set $T_i = \infty$ and $T_d = 0$. Initially set $K_p = 0$.

**Step 2:** Increase $K_p$ until there is a sustained oscillation (stability limit) in the output.

**Step 3:** This $K_p$ value is denoted the ultimate gain $K_u$. Measure the ultimate (or critical) period $P_u$ of the sustained oscillation.

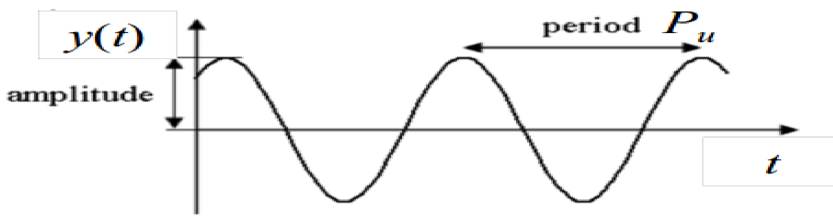


Figure 4.8:- Sustained oscillation of a plant (Smuts, 2011).

**Step 4:** Set the gains according to the Table 4.3 and tune finely in the vicinity if necessary.

Table 4.3:- Parameter calculation for ZN closed loop tuning method (Smuts, 2011).

| Controllers | Parameters | | |
|---|---|---|---|
| | $K_p$ | $T_i$ | $T_d$ |
| P | $0.5K_u$ | - | - |
| PI | $0.45K_u$ | $\frac{P_u}{1.2}$ | - |
| PID | $0.6K_u$ | $\frac{P_u}{2}$ | $\frac{P_u}{8}$ |

Using the expression of $U$ as shown below, the parameters of PID are adjusted using Equation (4.46).

$$U = K_p(1 + \frac{1}{T_i s} + T_d s) \tag{4.47}$$

From Equation (4.46),

$$K_p = K_p$$
$$K_i = \frac{K_p}{T_i} \tag{4.48}$$
$$K_d = K_p T_d$$

## 4.9 Overall System Structure

An Electrical Load Simulator's mathematical model is designed in state space form and transfer function. There are two subsystems in an Electrical Load Simulator structure. The two systems are the loading system and the loaded system. Without any controller, the loading system can't track its reference. Extra torque is added and output torque becomes very large. In order to track the output torque of this system, it needs a robust controller like STSMC. As shown in Figure 4.9 below, the system is a MIMO (two input, two output) system. The first input is the position of the tested actuator. The other input is the torque, which is used to simulate its equivalent aerodynamic load. This reference torque is proportional to aerodynamic load and is generated by the load calculator. Aerodynamic loads are introduced during flight at the control surfaces or fins of a flight vehicle. The output torque of the loading system is compared with the reference torque and fed to the controller, so that the controller reduces error or extra torque generated in this system. The controller parameters are tuned using the GWO algorithm in order to produce a satisfactory result. The overall system structure is shown in Figure 4.9 below.

The following are the primary characteristics of the proposed ELS conntroller:

a) The position of tested actuator is set at an angle of $\theta_{ref}(t) = 50\sin(2\pi t)\,rad$. Tested system used PID for position control of actuator (Tayyeb et al., 2021).

b) The output of the aerodynamic load calculator system serves as a reference command to the loading system. The inputs to the aerodynamic load calculator are the reference position command of the tested system, wind attack, air speed, match number, etc. For simplicity, the load calculator is used in proportional mode and considers only the reference position command of the tested system as an input to it. So the reference input to loading system is $T_{ref}(t) = C\theta_{ref} = 100 \sin(2\pi t)\,Nm$ by using proportional gain $C = 2$ (Shamisa & Kiani, 2018).

c) Nonlinear friction torque is modeled using LuGre model as shown in section 3.7.

d) In order to show the performance of controllers under different frequency variation,  frequency is selected as 1 Hz, 5 Hz and 10 Hz for this application (Zhang et al., 2021).

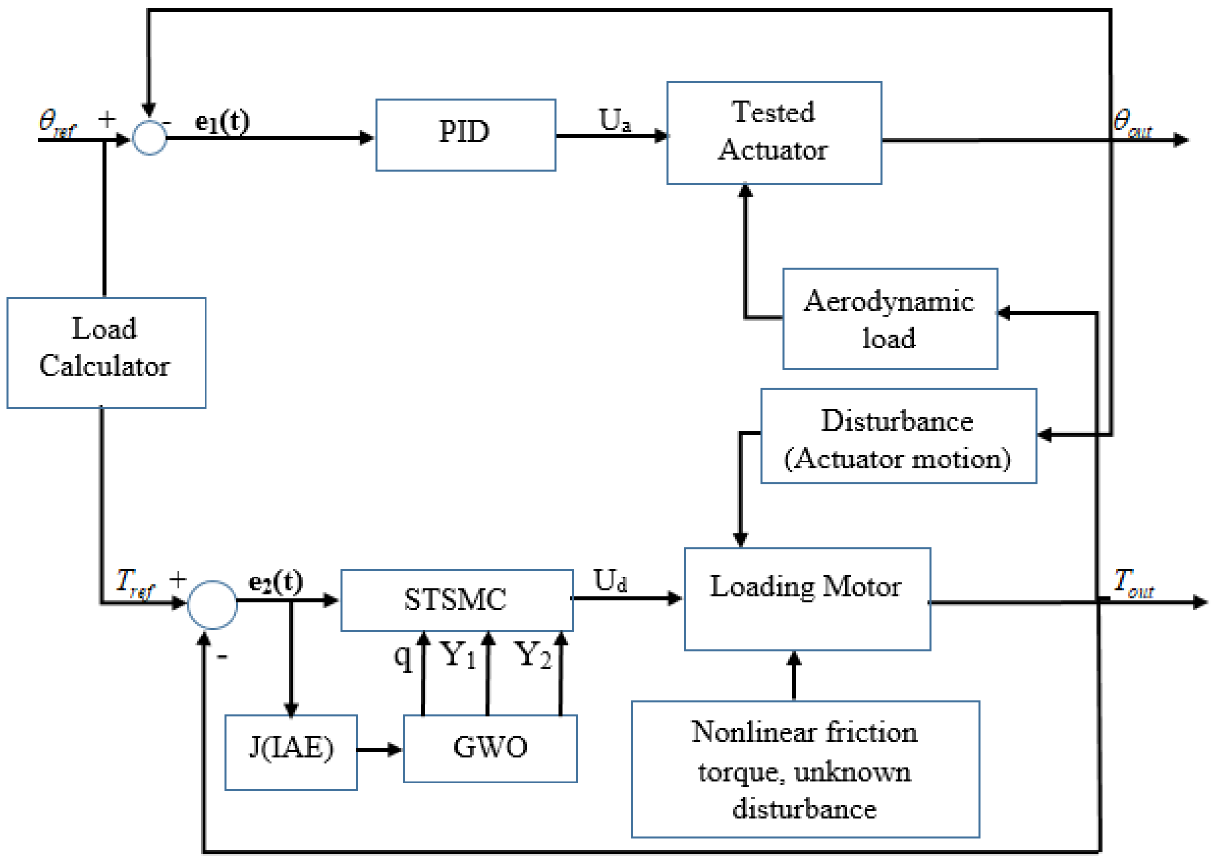


Figure 4.9:- Overall system structure.

The boundary of tuned parameters of Super twisted sliding mode control (STSMC) and PID are shown in Table 4.4 below.

Table 4.4:-  Boundary of tuned parameters of controllers for loading system.

| Boundary | STSMC-GWO | | | PID-GWO | | |
|---|---|---|---|---|---|---|
| | *q* | $Y_1$ | $Y_2$ | *Kp* | *Ki* | *Kd* |
| Lower bound | 0.0001 | 0.0001 | 0.0001 | 0.0001 | 0.0001 | 0.0001 |
| Upper bound | 10 | 15 | 30 | 25 | 15 | 10 |

The control parameters are adjusted using the GWO in relation to the proposed cost function (J). The tuning ranges for the parameters are determined as shown in Table 4.4, and the parameters for the suggested algorithm are listed in Table 4.5.

Table 4. 5:- Parameters of GWO algorithm for loading system.

| Algorithm | Parameter of Algorithm | |
|---|---|---|
| GWO | Number of search agent | 20 |
| | Maximum iteration | 20 |

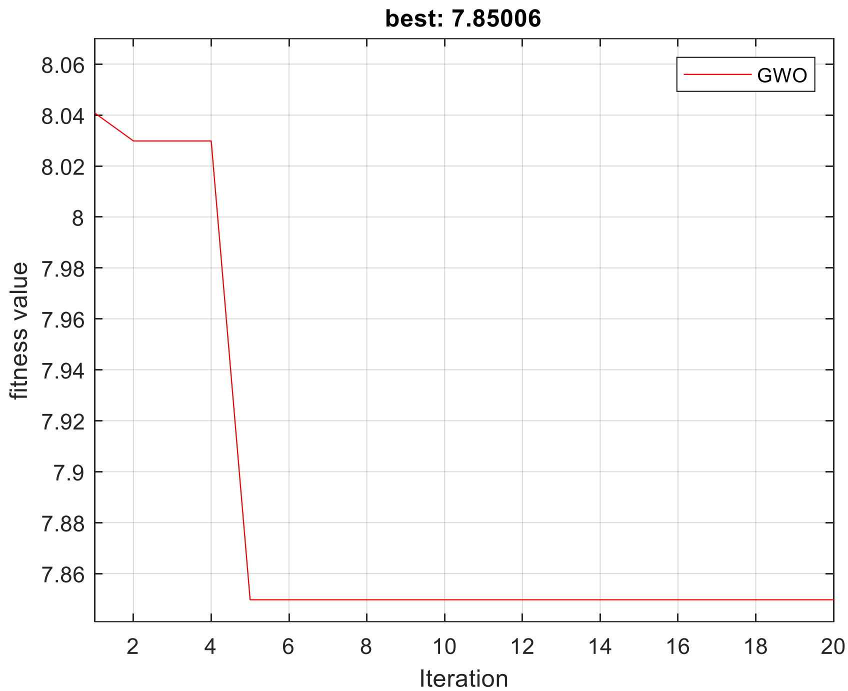


Figure 4.10:- Convergent curve of GWO in STSMC controller.

Figure 4.10 and 4.11 shows the convergence curve of the GWO in STSMC and PID controller. This graph clearly shows that GWO outperforms better in STSMC in terms of response by reducing the cost function more.

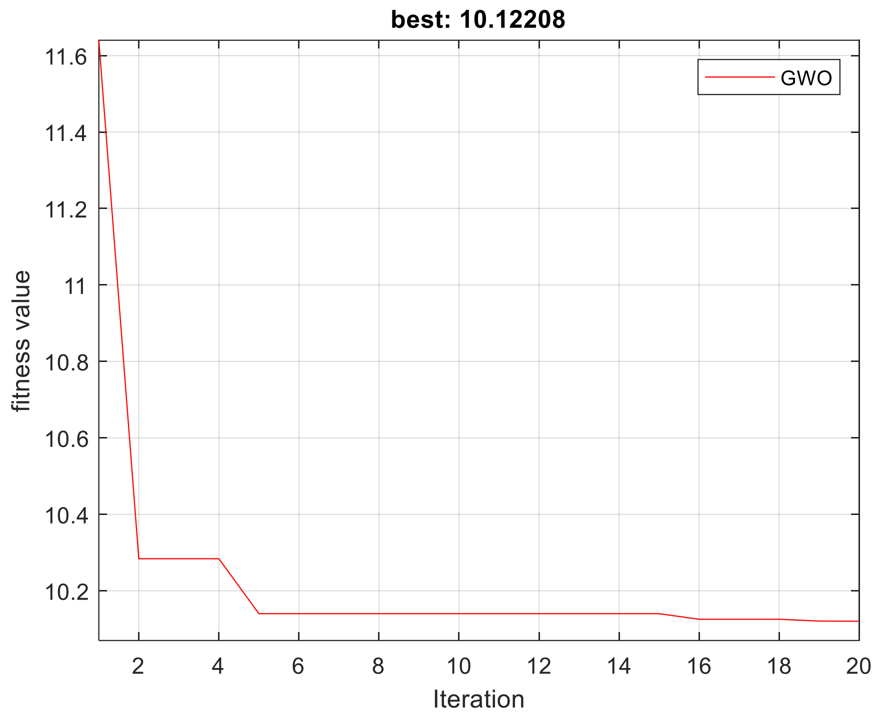


Figure 4.11:- Convergent curve of GWO in PID controller.

Table 4.6:- Optimal value of STSMC and PID controller for loading motor.

| Controller | Parameters | GWO |
|---|---|---|
| STSMC | $q$ | 3.75 |
| | $Y_1$ | 12.5 |
| | $Y_2$ | 26.74 |
| PID | $K_p$ | 22.53 |
| | $K_i$ | 10.3 |
| | $K_d$ | 5.82 |

Table 4.6 shows the optimal values of STSMC and PID parameters after tuning, corresponding to the minimum cost function value provided by the optimal GWO.

The parameters of conventional PID is determined by Ziegler-Nichols closed loop tuning. According to the steps provide in section 4.8.2 the parameters are determined from sustained oscillation.

Figure 4.12 indicate the sustained oscillation at ultimate gain $K_u$ = *58.5*. The ultimate period can be determined from the figure as $P_u$ =4.63-2.7= 1.93. Using the value of $K_u$ and $P_u$ the value of PID parameters are determined based on Table 4.3 and equation 4.48.

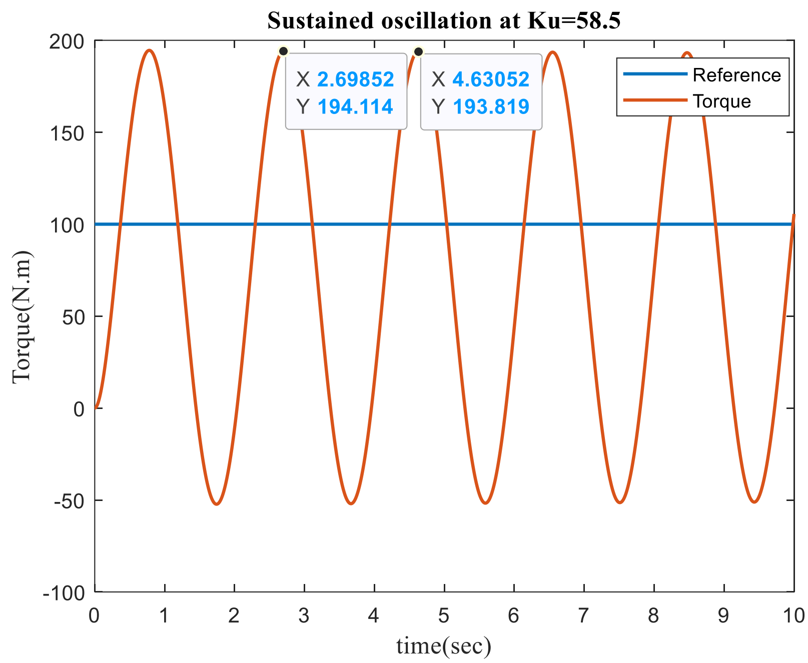


Figure 4.12:- Sustained oscillation.

Table 4.7:- Gain parameters using ZN closed loop tuning method.

| **Controllers** | **Parameters** | | |
|---|---|---|---|
| | $K_p$ | $T_i$ | $T_d$ |
| PID | 35.1 | 0.965 | 0.241 |

# CHAPTER FIVE

# 5. RESULTS AND DISCUSSIONS

## 5.1 Introduction

In this chapter, simulation was carried out using MATLAB/Simulink and code to verify the performance of the controller for an Electric Load Simulator system and to compare output result of GWO tuned STSMC (GWO-STSMC) with that of Grey Wolf Algorithm tuned PID controller (GWO-PID) and Ziegler-Nichols tuned PID (ZN-PID) controller. The trajectory tracking performance for three controllers was tested. The step response of an Electric Load simulator was also performed for three controllers.

The open_loop dynamic model of the plant simulation was performed based on the parameters of an Electric Load Simulator in Tables 3.1 and 3.2. An open_loop dynamic model of an Electric Load Simulator is created in MATLAB/Simulink as shown in Figure 5.1.

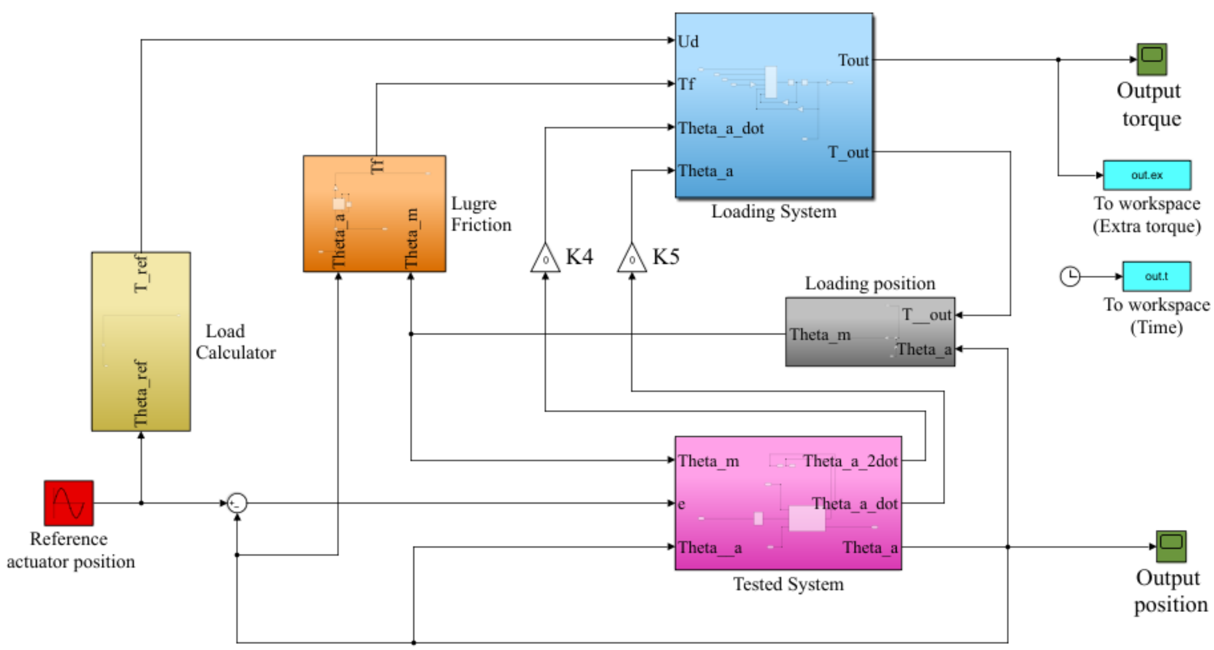


Figure 5.1:- MATLAB/Simulink open_loop dynamic model of an Electric Load Simulator.

Some description of the MATLAB/Simulink model in Figure 5.1.

a) The light blue color shows the loading system.
b) The magenta color shows a loaded system or tested system which was tested by applying aerodynamic load (i.e., loading torque).
c) The orange color shows modeled nonlinear friction torque disturbance.
d) The yellow color show load calculator which generates reference input for loading system based on reference command of the tested actuator.

As shown in Figure 5.1, there are two subsystems, i.e., the loading subsystem and the loaded subsystem. The loading subsystem is a system that generates aerodynamic load and applies this aerodynamic load to the loaded system for testing and qualification purposes as described in the above sections. Aerodynamic load (loading torque) from this subsystem must be controlled for accurate testing and qualification of the tested system. The loaded subsystem was taken from (Tayyeb et al., 2021), which was going to be tested. The main challenge in the loading subsystem is to eliminate extra torque. Extra torque is caused by the effect of motion of the tested system (i.e., $\theta$, $\dot{\theta}$ and $\ddot{\theta}$ ) , friction torque disturbance and unknown disturbance.

The result for the open_loop dynamic model of the plant is illustrated as shown in the following conditions:

a) Set ELS desired loading torque ($T_{ref}(t)$) zero and the actuator operates with a desired sinusoidal position command (i.e., $\theta_{ref}(t) = 50\sin(2\pi t)$) rad, then the measured torque output of loading system is so-called extra torque. The total extra torque produced in an Electric Load Simulator due to the effect of actuator motion, friction torque disturbance, and unknown disturbances is shown in Figure 5.2 below.

   From Figure 5.2, a large extra torque is produced due to the effect of the motion of the actuator, friction torque disturbance, and unknown disturbances at the frequency of 1 Hz actuator motion. This large extra torque affects the testing and qualification of the actuator. The maximum amplitude of this large extra torque is 22.16 N.m, which can be found using the MATLAB command max(out. ex).

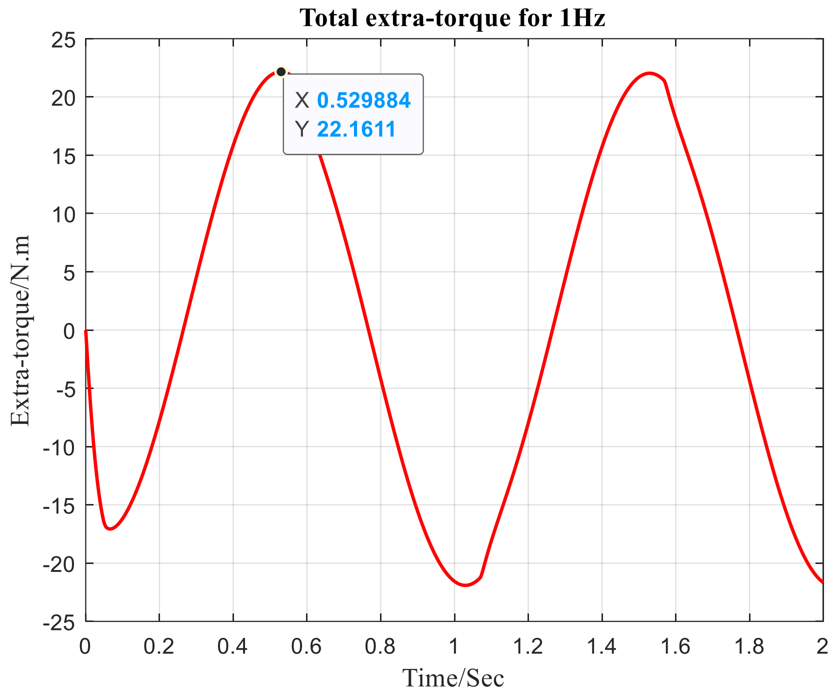


Figure 5.2:- Total Extra torque.

b) In order to know the contribution of the motion of the actuator and unknown disturbances only for the addition of extra torque (i.e., without friction torque disturbance), set ELS desired loading torque ($T_{ref}(t)$) zero, desired sinusoidal position command ($\theta_{ref}(t)$) $50\sin(2\pi t)$ rad, and friction torque disturbance ($T_f(t)$) zero, then measure torque output (extra-torque) of loading system. The extra torque produced due to the effect of motion of actuator's and unknown disturbance is shown in Figure 5.3 below. The maximum amplitude of extra-torque occurred at 1 Hz actuator motion due to the effect of the motion of the actuator and unknown disturbances only is 19.84 N.m.

c) To analyze the effect of friction torque disturbance and unknown disturbance only for the addition of extra torque (i.e., ignoring the effect of motion of actuator to be tested), set ELS desired loading torque ($T_{ref}(t)$) zero, desired sinusoidal position command ($\theta_{ref}(t)$) 50 $\sin(2\pi t)$ rad and actuator motion ($\ddot{\theta}_a(t) = \dot{\theta}_a(t)$) zero, then measure the torque output of loading system. The extra torque produced due to the effect of friction torque disturbance and unknown disturbance only is shown in Figure 5.4 below. The maximum amplitude of extra torque occurred at 1 Hz actuator motion due to such effect is 3.10 N.m.

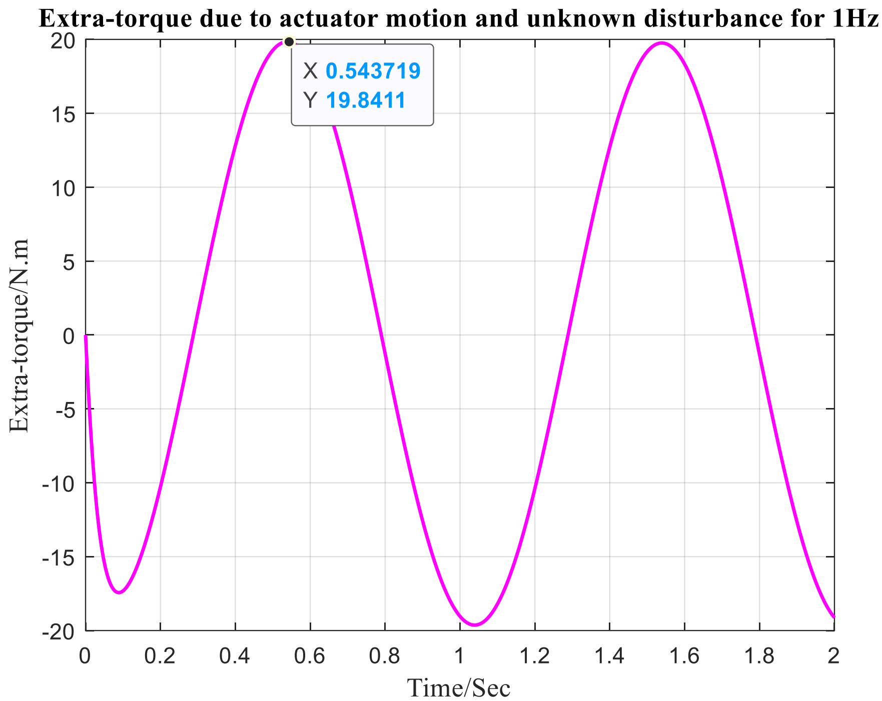


Figure 5.3:- Extra torque produced due to the motion of actuator and unknown disturbance only.

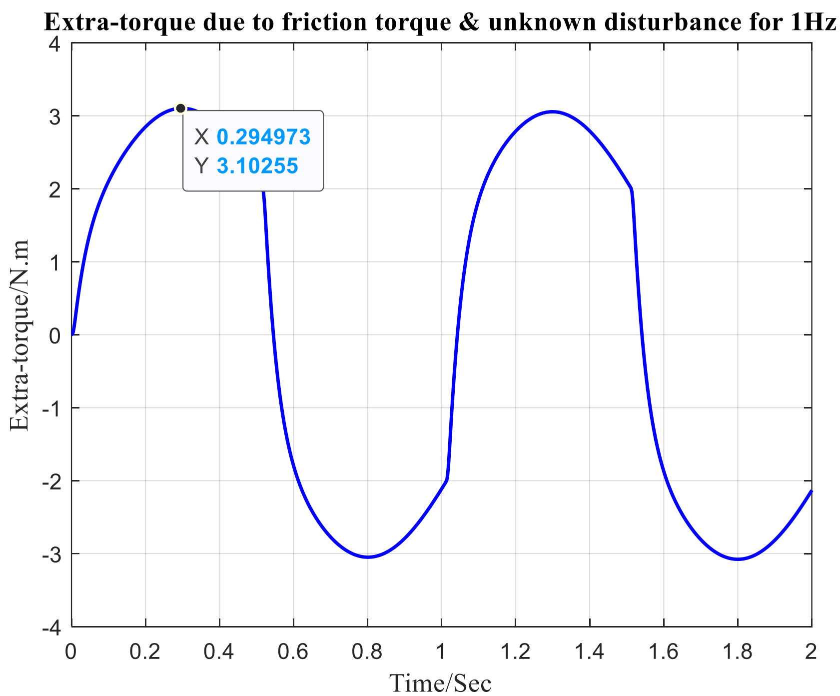


Figure 5.4:- Extra torque produced due to friction torque disturbance and unknown disturbance only.

Generally, the effect of each disturbance acting on an Electric Load Simulator for the addition of extra torque can be summarized using simple calculation as illustrated below.

Assume the extra torque caused by the actuator's motion is $M_d$, the extra torque caused by an unknown disturbance is $U_d$, and the extra torque caused by a friction torque disturbance is $F_d$. Therefore, the maximum amplitude of extra torque caused by these effects at 1 Hz actuator motion is:

$$M_d + U_d = 19.84 N.m \tag{5.1}$$

$$F_d + U_d = 3.10 N.m \tag{5.2}$$

Total extra-torque occurred is expressed as:

$$M_d + U_d + F_d = 22.16 N.m \tag{5.3}$$

Then by substituting Equation (5.1) to Equation (5.3):

$$19.84 N.m + F_d = 22.16 N.m$$

$$F_d = 2.32 N.m \tag{5.4}$$

Using Equation (5.1) and Equation (5.2) the maximum amplitude of extra-torque occurred due to $M_d$ is 19.06N.m and due to $U_d$ is 0.78N.m. The maximum amplitude of extra torque due to each effect is summarized in Table 5.1 below.

Table 5.1:- Extra torque occurred due to disturbances at 1Hz.

| | Disturbances | | |
|---|---|---|---|
| | Motion of tested actuator | Friction torque disturbance | Unknown disturbance |
| Max. amplitude (N.m) | 19.06 | 2.32 | 0.78 |
| Total extra-torque Max. amplitude (N.m) | 22.16 | | |

As shown in Table 5.1, the extra-torque that occurred due to the effect of the motion of the tested actuator is large compared to the friction torque disturbance and unknown disturbance in 1Hz actuator motion. So the motion of the tested actuator is the main contributor to the occurrence of extra-torque. Extra-torque caused by an unknown disturbance is insignificant in comparison to the motion of the tested actuator and friction torque disturbance. Extra-torque occurred due to each effect is plotted in one figure as shown in Figure 5.5.

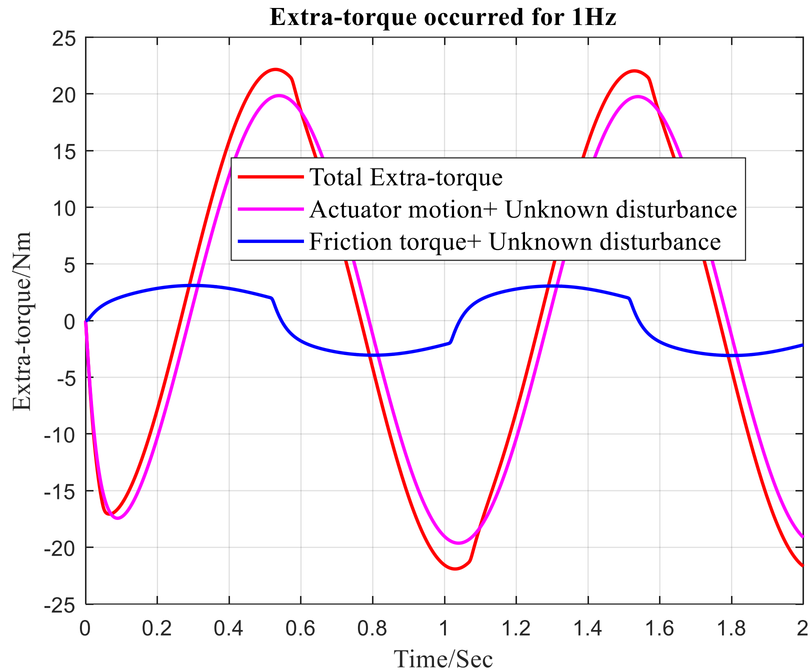


Figure 5.5:- Extra-torque due to each effect in one plot at 1 Hz.

d) As the frequency of motion of the tested actuator increases, the extra-torque occurred in an Electrical Load Simulator increase. In addition, similar to low frequency (i.e., 1 Hz) the motion of the tested actuator has a large effect on the occurrence of extra-torque, and unknown disturbances have a very small effect on the occurrence of extra-torque as the frequency increases. To show the effect of frequency on the occurrence of extra-torque and to show the effect of each disturbance on the occurrence of extra-torque, the frequency of the desired sinusoidal position command (i.e. $\theta_{ref}(t) = 50\sin(2\pi t)\,\mathrm{rad}$) is varied from 1Hz to 5Hz and 10Hz.

Table 5.2:- Extra-torque occurred due to disturbances at 5Hz.

| | Disturbances | | |
|---|---|---|---|
| | Motion of tested actuator | Friction torque disturbance | Unknown disturbance |
| Max. amplitude (N.m) | 63.23 | 9.49 | 0.98 |
| Total extra-torque amplitude (N.m) | 73.70 | | |

As shown in Figure 5.6 and Table 5.2, similar to 1 Hz actuator motion, the effect of actuator motion has a large effect on the occurrence of extra-torque at 5 Hz. Similarly, unknown disturbance has very small effect on the occurrence of extra-torque compared to the motion of the actuator and friction torque disturbance.

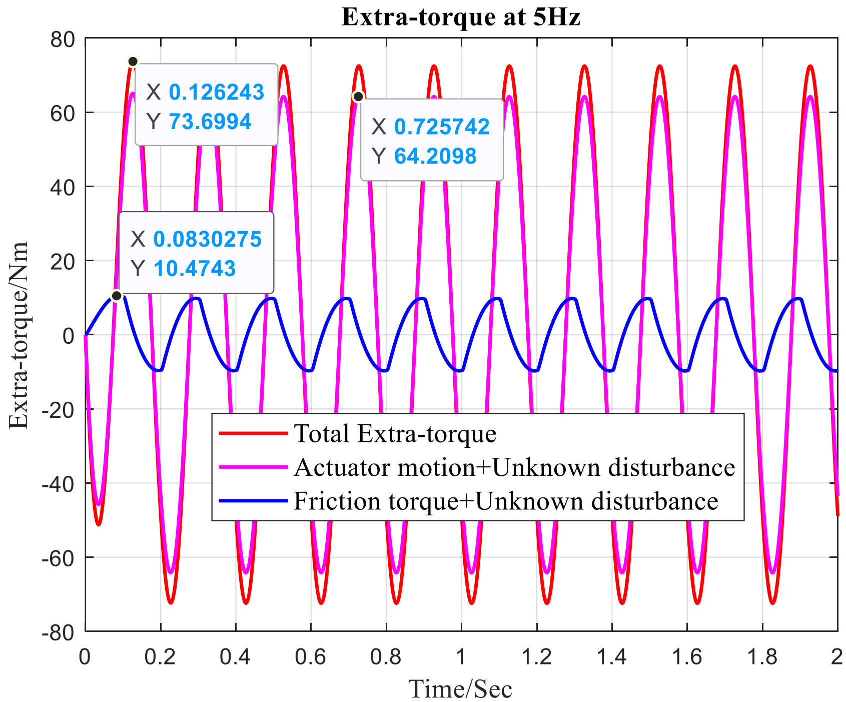


Figure 5.6:- Extra-torque at 5Hz.

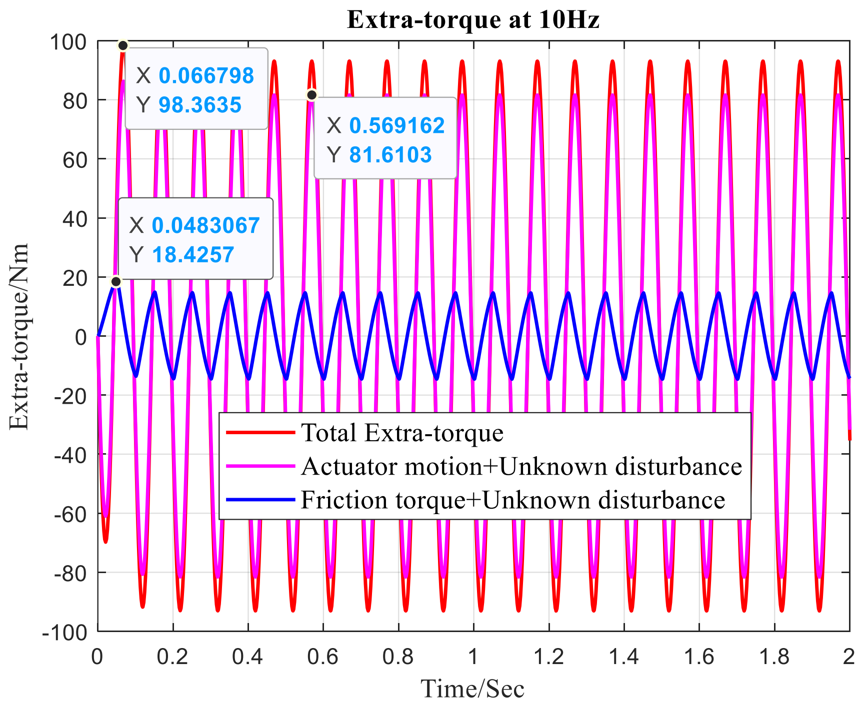


Figure 5.7:- Extra-torque at 10Hz.

Table 5.3:- Extra-torque occurred due to disturbances at 10Hz.

| | Disturbances | | |
|---|---|---|---|
| | Motion of tested actuator | Friction torque disturbance | Unknown disturbance |
| Max. amplitude (N.m) | 79.93 | 16.75 | 1.68 |
| Total extra-torque amplitude (N.m) | 98.36 | | |

As shown in Figure 5.7 and Table 5.3 above, large extra torque occurs in an Electrical Load Simulator at 10 Hz actuator motion. Similar to 1 Hz and 5 Hz actuator motion, large extra torque occurs due to actuator motion and small extra torque occurs due to unknown disturbance. The extra torque produced in 10 Hz actuator motion is large compared to 1 Hz and 5 Hz actuator motion. This indicate that the extra torque occurred in ELS is affected by frequency.

Table 5.4:- Summary of extra torque at different frequency.

| | Frequency | | |
|---|---|---|---|
| | 1Hz | 5Hz | 10Hz |
| Total extra-torque max. amplitude (N.m) | 22.16 | 73.70 | 98.36 |

Table 5.4 shows that extra-torque occurring in an Electrical Load Simulator increases as the frequency of the motion of the actuator increases.

Generally, the open loop response of an Electrical Load Simulator indicates a large extra torque has occurred due to the motion of the tested actuator, nonlinear friction torque, and unknown disturbances. The motion of the tested actuator creates more extra torque compared to nonlinear friction disturbance and unknown disturbance. The effect of an unknown disturbance is very small compared to the effect of motion of the tested actuator and friction torque disturbance. Extra torque produced in an Electrical Load Simulator increases as the loading frequency increases. This extra torque is very large and may even be greater than the desired loading torque. As a result, without applying any controller to an Electrical Load Simulator, it is difficult to use an Electrical Load Simulator for testing and qualification of actuator. It is difficult to compensate for it using a conventional controller. Using a robust controller reduces the occurrence of extra torque in an Electrical Load Simulator.

## 5.2 Simulation Results

The loading torque of the loading system is controlled with Grey Wolf Optimization based STSMC to reduce the extra torque added to the shaft of the loading motor. For the purpose of comparison, Ziegler-Nichols tuned PID and Grey Wolf Optimization tuned PID are used. The performance of these controllers are evaluated based on the value of integral absolute error (IAE) for the sine reference input. These controllers are also compared in terms of time domain sepecification for step reference input.

Set the desired position trajectory of the actuation system as $\theta_{ref}(t) = 50\sin(2\pi t)$ rad and, from the load calculator, the desired loading torque of ELS became $T_{ref}(t) = 100\sin(2\pi t)$ N.m. First, ELS is operated using GWO tuned STSMC and then ELS is operated with GWO and ZN tuned PID for the purpose of comparison. The trajectory tracking and tracking error of these controllers for 1 Hz motion of the actuation system are shown in Figure 5.8 and 5.9, respectively.

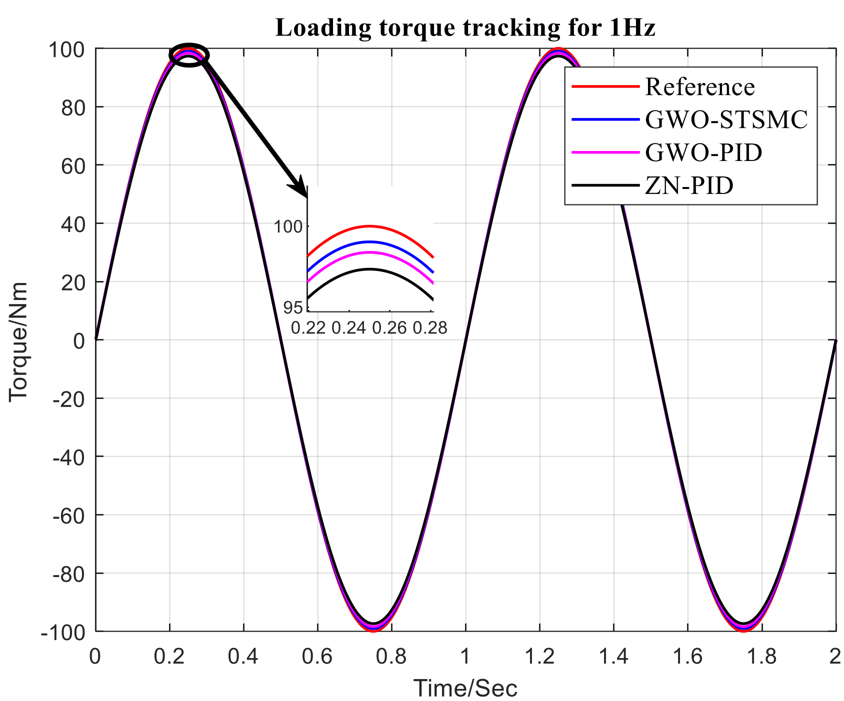


Figure 5.8:- Loading torque Tracking of ELS for 1Hz.

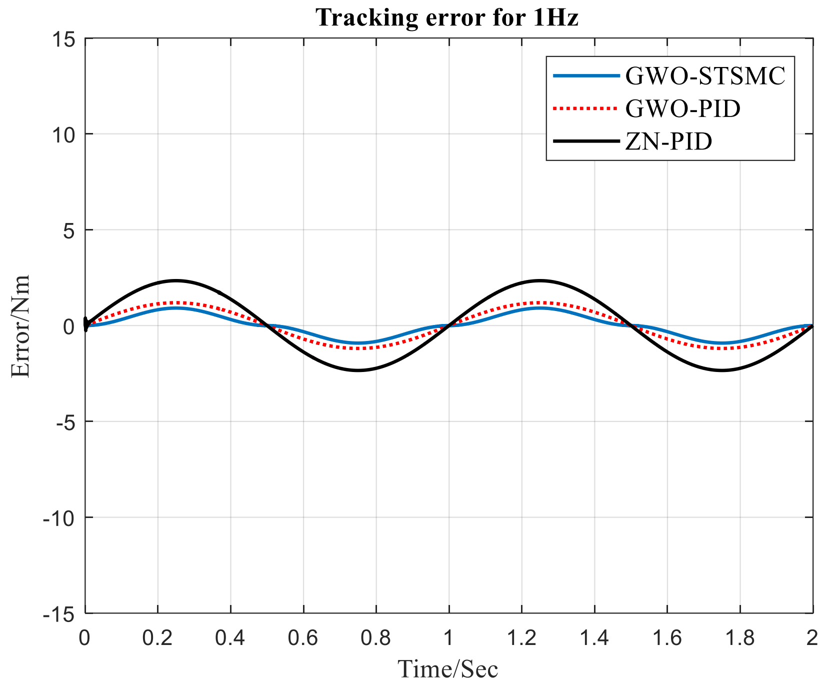


Figure 5.9:- Tracking error of controllers for 1Hz.

According to Figures 5.8 and 5.9, GWO tuned STSMC has excellent performance in eliminating extra torque compared to ZN tuned PID and GWO tuned PID. The large extra-torque occurred in ELS is difficult to eliminate using conventional PID, as shown in Figures 5.8 and 5.9. In order to intuitively compare the effects of the designed controllers, the extra torque (tracking error) quantitative index (IAE) is introduced here:

$$IAE = \int_{0}^{t_f} |e(t)|\, dt \tag{5.5}$$

Among them: *e(t)* is the dynamic loading of the excess torque; $t_f$ is taken as 10s; IAE is integral absolute error, and the smaller the value, the better the suppression of the extra torque. Equation (5.5) can be easily computed using Simulink as shown in Figure 5.10 below.

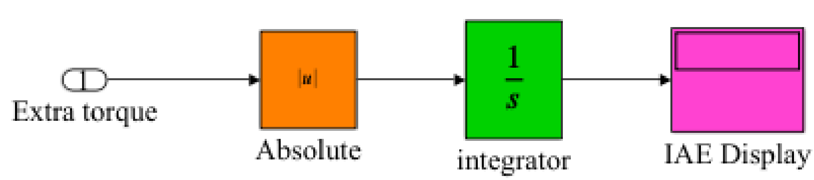


Figure 5.10:- IAE calculator.

According to Equation (5.5), the IAE value of tracking error for three controllers and the maximum amplitude of tracking error for three controllers at 1Hz loading frequency is shown in Table 5.5 below.

Table 5.5:- IAE and maximum amplitude of tracking error for the three controllers at 1Hz.

| | Controller | | |
|---|---|---|---|
| | GWO-STSMC | GWO-PID | ZN-PID |
| IAE | 7.85 | 10.12 | 19.29 |
| Max-amplitude (N.m) | 0.95 | 1.22 | 2.34 |

The value of IAE and maximum amplitude of tracking error in Table 5.5 indicate that the GWO-tuned STSMC controller has the best suppression ability of the extra torque. Optimization-based PID is better than conventional PID for the suppression of extra torque. After adopting the GWO-STSMC controller designed in this paper, the suppression of the residual torque at 1Hz is improved by 59.31% as compared with ZN-PID and by 22.43% as compared with GWO-PID. The GWO-PID and GWO-STSMC have the best performance at eliminating extra torque in this condition. In addition, GWO-STSMC is more effective than GWO-PID.

Figure 5.11 indicates trajectory tracking of ELS at 5 Hz using three control strategies. Figure 5.12 indicates the tracking error of loading torque. It is clearly seen in Figures 5.11 and 5.12 that GWO-STSMC performances best at eliminating extra torque as the loading frequency increases. The tracking performance of GWO-STSMC is best compared to the two controllers. Additionally, as shown in Figure 5.12 below, the tracking error of GWO-STSMC is minimum when compared to GWO-PID and ZN-PID. Due to the effect of optimization, the GWO-PID controller has best performance compared to the ZN-PID at 1 Hz loading frequency. According to an open-loop analysis of the ELS, the extra torque that occurs at the 5 Hz loading frequency is very large in comparison to 1 Hz.This large extra-torque is reduced too much by using the GWO-STSMC controller. In order to quantitatively compare the performance of the designed controllers, the IAE and maximum amplitude of extra-torque (tracking-error) are expressed in Table 5.6 below.

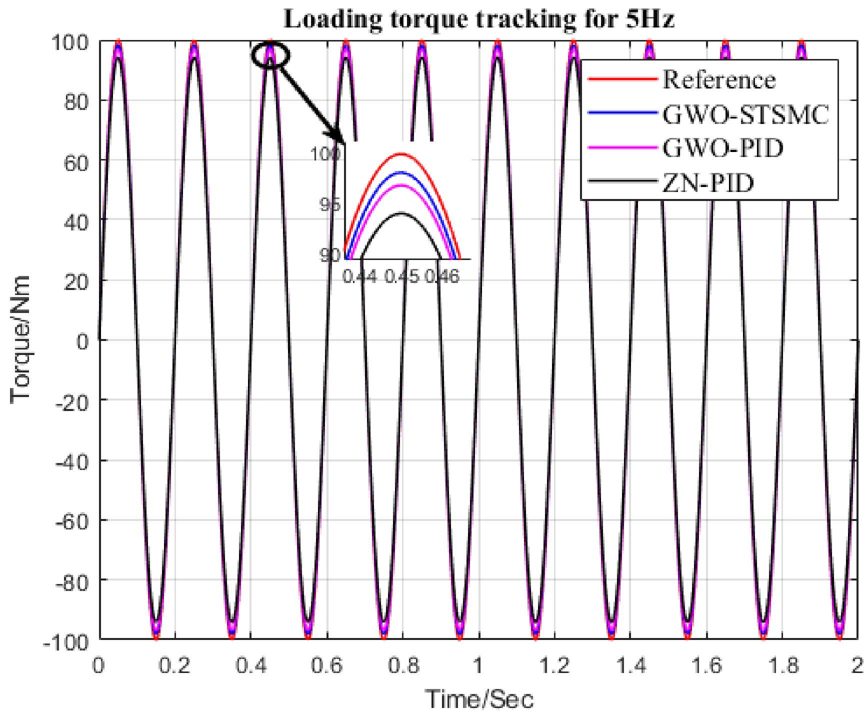


Figure 5.11:- Loading torque Tracking of ELS at 5Hz.

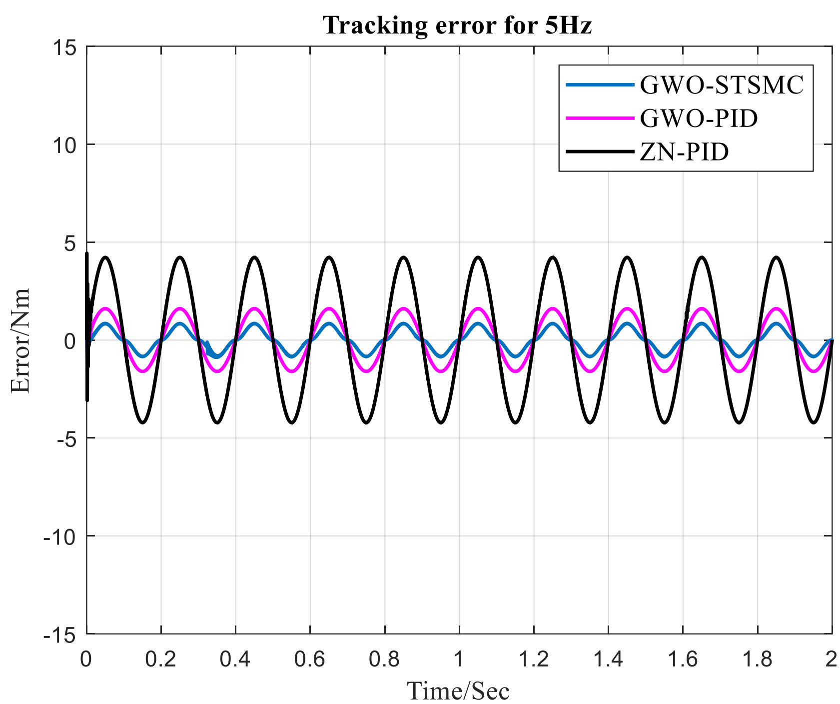


Figure 5.12:- Tracking error of three controllers at 5Hz.

Table 5.6:- IAE and maximum amplitude of tracking error for the three controllers at 5Hz

| | Controller | | |
|---|---|---|---|
| | GWO-STSMC | GWO-PID | ZN-PID |
| IAE | 37.36 | 50.01 | 134.67 |
| Max-amplitude (N.m) | 1.23 | 1.64 | 4.43 |

After adopting the GWO-STSMC controller designed in this paper, the suppression of the residual torque at 5 Hz is improved by 72.26% as compared with ZN-PID and by 25.30% as compared with GWO-PID. The value of IAE and maximum amplitude of tracking error in Table 5.6 indicate that GWO-STSMC and GWO-PID have better suppression ability of tracking error at 5Hz loading frequency. GWO-STSMC is the best at eliminating extra torque from the two controllers.

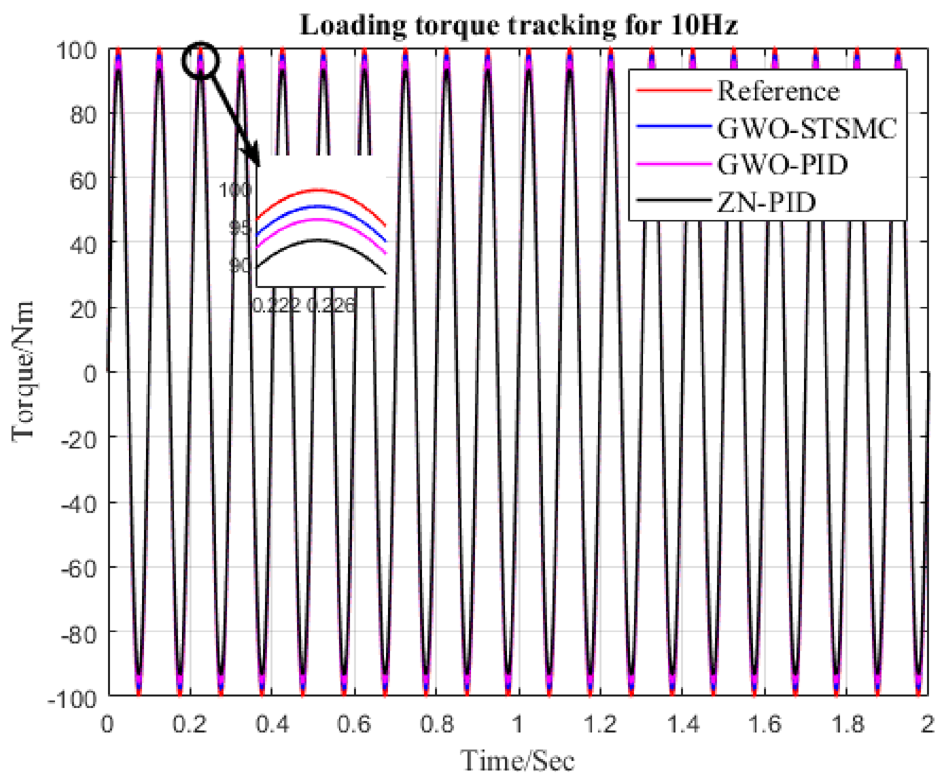


Figure 5.13:- Loading torque Tracking of ELS at 10 Hz.

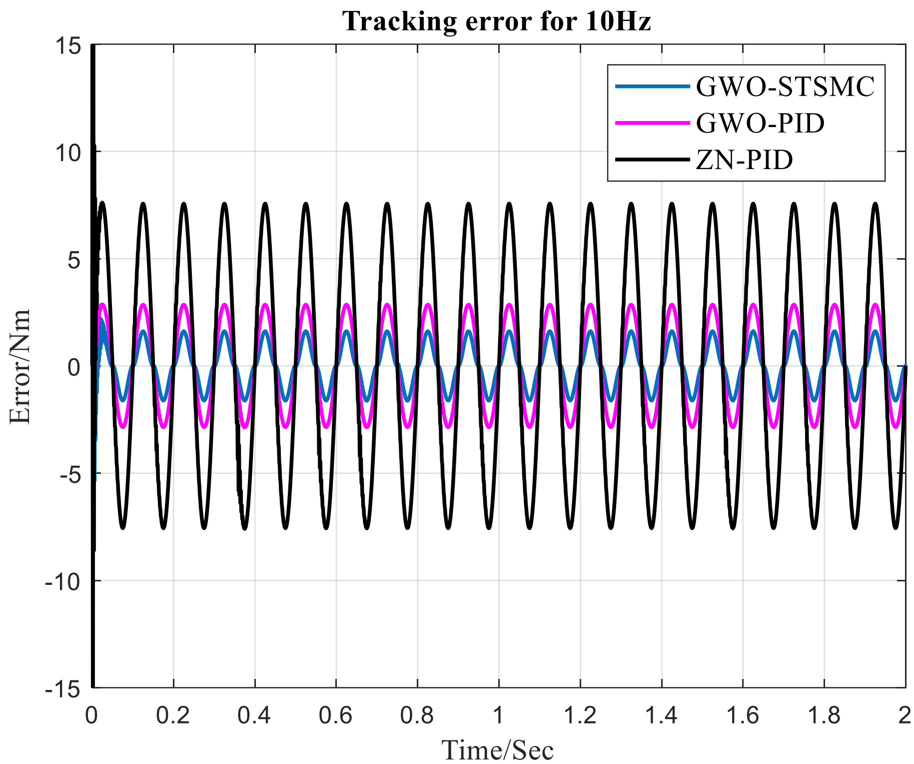


Figure 5.14:- Tracking error of ELS at 10 Hz.

Table 5.7:- IAE and maximum amplitude of tracking error for the three controllers at 10 Hz.

| | Controller | | |
|---|---|---|---|
| | GWO-STSMC | GWO-PID | ZN-PID |
| IAE | 70.99 | 98.83 | 374.95 |
| Max-amplitude (N.m) | 1.62 | 2.26 | 8.56 |

As shown clearly in Figures 5.13, 5.14, and Table 5.7, even though the amount of extra torque occurred in an Electric Load Simulator increases as the frequency increases, the suppression ability of GWO-STSMC increases as compared to ZN-PID and GWO-PID controllers. After adopting the GWO-STSMC controller designed in this paper, the suppression of the extra torque at 10 Hz is improved by 81.07% as compared with ZN-PID and 28.17% as compared with GWO-PID.

Table 5.8:- Summary of controller IAE and maximum amplitude value at different frequencies

| Controller | Loading frequency | | | | | |
|---|---|---|---|---|---|---|
| | 1Hz | | 5Hz | | 10Hz | |
| | IAE | Max.amp (N.m) | IAE | Max.amp (N.m) | IAE | Max.amp (N.m) |
| ZN-PID | 19.29 | 2.34 | 134.67 | 4.43 | 374.95 | 8.56 |
| GWO-PID | 10.12 | 1.22 | 50.01 | 1.64 | 98.83 | 2.26 |
| GWO-STSMC | 7.85 | 0.95 | 37.36 | 1.23 | 70.99 | 1.62 |
| Extra-torque suppression rate of GWO-STSMC compared with ZN-PID | 59.31% | | 72.26% | | 81.07% | |
| Extra-torque suppression rate of GWO-STSMC compared with GWO-PID | 22.43% | | 25.30% | | 28.17% | |

As shown in Table 5.8, we can conclude that the GWO-STSMC controller has best performance in eliminating extra-torque caused by the motion of the tested actuator, nonlinear friction torque disturbance, and unknown disturbance as compared with ZN-PID and GWO-PID. As the loading frequency increases, the extra torque that occurs in ELS increases too much. This large extra torque that occurs in the loading system is difficult to eliminate using conventional PID, as shown in the above results. This excess extra torque in the ELS is effectively reduced by GWO-STSMC. The extra-torque suppression rate in Table 5.8 above indicates the performance of this controller is also best as loading frequency increases.

In order to know the performance of the designed controller in terms of time domain specification, step response analysis is required. Step value of 100 N.m was applied as loading torque. Figure 5.15 and 5.16 indicate the tracking performance of three controllers and tracking error, respectively. According to the result, GWO-STSMC has a better response in terms of time domain specification than GWO and ZN tuned PID, as shown in Table 5.9. Rise time ($t_r$), settling time ($t_s$) and overshoot ($M_p$) are improved well by using GWO-STSMC as compared with GWO-PID and ZN-PID. This indicates that the GWO-STSMC controller is best in eliminating extra torque that occurs in ELS. GWO-PID is better than ZN-PID due to the role of optimization.

Table 5.9:- Time domain performance of the three controllers

| Performance | GWO-STSMC | GWO-PID | ZN-PID |
|---|---|---|---|
| $t_r$ (sec) | 0.08 | 0.13 | 0.22 |
| $t_s$ (sec) | 0.78 | 1.17 | 1.49 |
| $M_p$ (%) | 4.24 | 9.32 | 15.21 |

Figure 5.15 show the step response of the Electric Load Simulator using the ZN-PID, GWO-PID and GWO-STSMC controllers. The tracking performance of GWO-STSMC is also best in the step response.

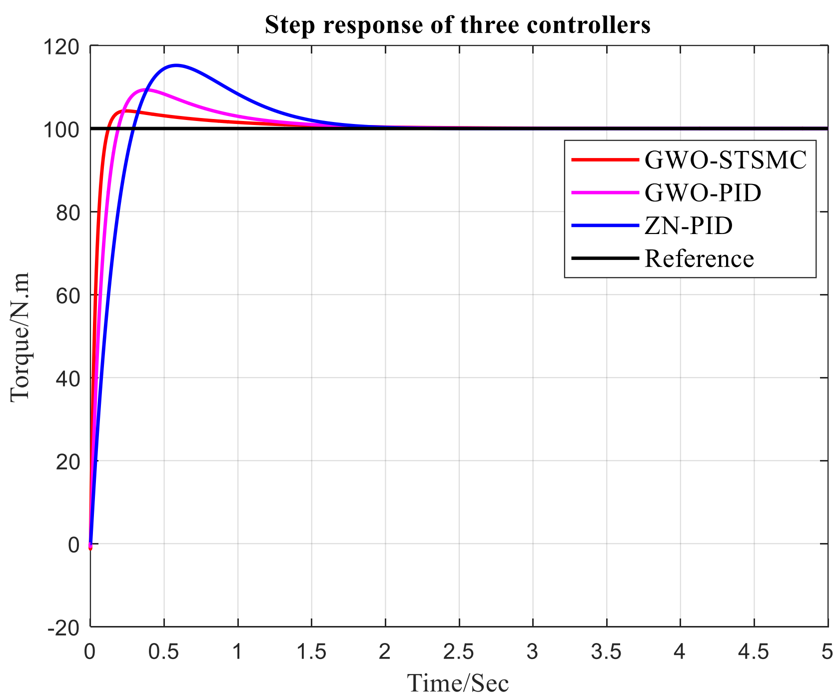


Figure 5.15:- Step response of ELS for three controller.

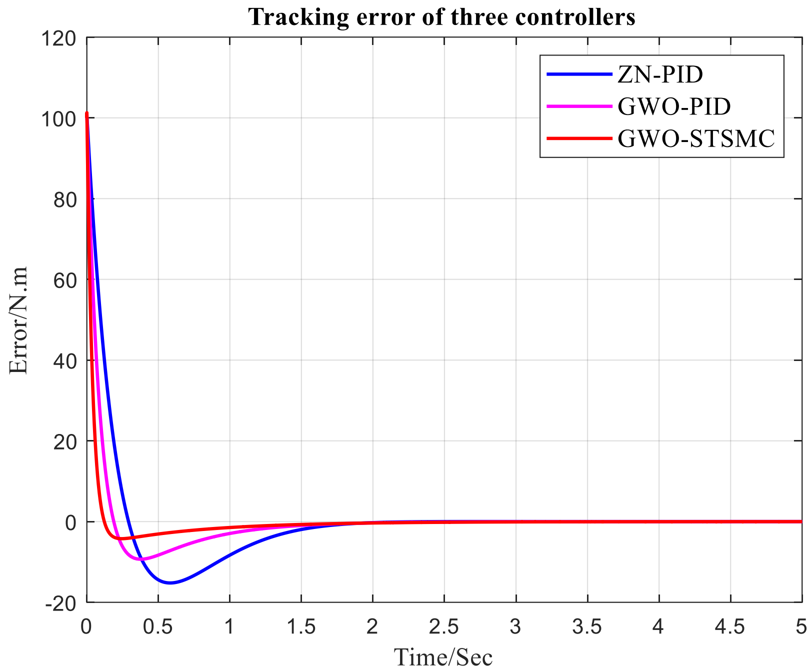


Figure 5.16:- Tracking error of ELS for step response.

The proposed controller's performance is also evaluated using random signals to demonstrate controller performance under unexpected variations in ELS reference input, such as wind guest. Figure 5.17 shows the tracking performance of the three controllers.

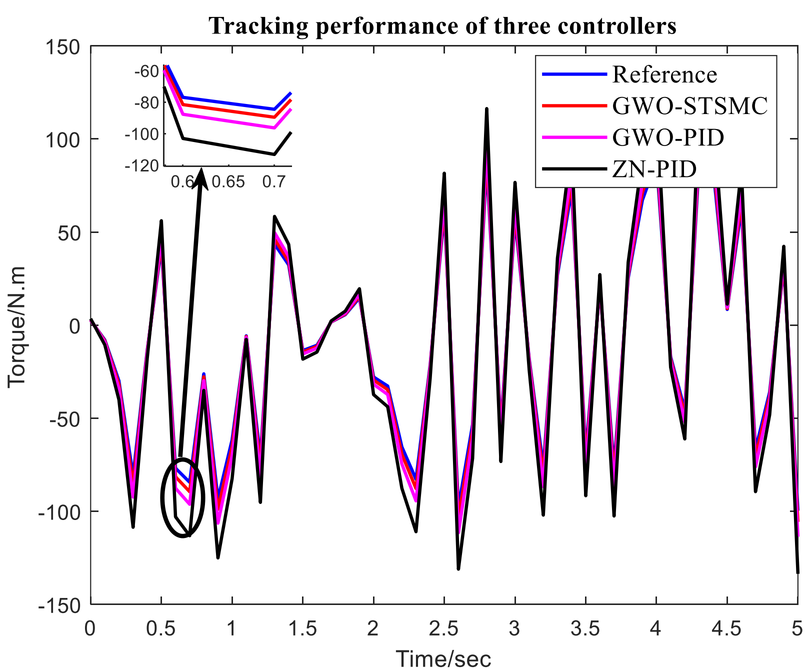


Figure 5.17:- Tracking performance of ELS for random signal.

The GWO-STSMC performs well for random reference signals, as shown in Figure 5.17. so that GWO-STSMC has the best tracking performance for different variations of the input reference signal.

In general, an Electric Load Simulator is effectivly controlled through reference sine input, step reference input and rondom reference signal and all simulation results show that ELS can operate with good performance using the GWO-STSMC and GWO-PID controller. The GWO-STSMC controller is best compared to GWO-PID and ZN-PID. As a result, by using GWO-STSMC controller, ELS can be efficiently used for testing and qualification of the actuators of an aircraft elevator.

# 6. CONCLUSIONS AND RECOMMENDATIONS

## 6.1 Conclusions

The Electric Load Simulator is one of the main mechanisms for stability and performance evaluation of the rotational and translational actuators in the laboratory. The movement of the (under testing) actuator, friction torque disturbance, and unknown disturbance generate a large extraneous torque on the load simulator, as shown in the result of open loop response. This large extra torque is increased too much as the loading frequency increases. Elimination of this large surplus disturbance is the main concern of an Electric Load Simulator design.

In this paper, a Super Twisted Sliding Model Controller (STSMC) method has been proposed for loading torque control of an Electric Load Simulator. A PID controller is used for performance comparison of the STSMC controller. The tested system is the actuator of an aircraft elevator, which is taken from literature. The friction torque disturbance is modeled using the LuGre friction model. The mathematical models of the loading and loaded systems are driven in state space and transfer function and designed in MATLAB/Simulink.

The parameters of the STSMC controller used in this work are tuned using Gray Wolf Optimization (GWO). The PID controller parameters are tuned using both the Ziegler-Nichols (ZN) method and Grey Wolf Optimization (GWO*)*. The Grey Wolf Optimization tuned STSMC (GWO-STSMC) controller has the best tracking performance at low loading frequencies as well as when the loading frequency increases as compared to the Ziegler-Nichols tuned PID (ZN-PID) and Grey Wolf Optimization tuned PID (GWO-PID) controllers. The simulation results show that, compared with conventional PID control and GWO-PID, the GWO-STSMC can effectively reduce the large excess torque and improve the loading accuracy of the system. To evaluate the controller's performance in terms of time domain specification, step reference input is used. The GWO-STSMC controller also has better performance than ZN-PID and GWO-PID in terms of time domain specification. It has a rise time of 0.08 sec, a settling time of 0.78 sec, and an overshoot of 4.24%. The GWO-STSMC also performs well for random reference signals and has the best tracking performance for different variations of the input reference signal. Finally, simulation results demonstrate that an Electric Load Simulator based on GWO-STSMC performes well and can be used for testing and qualification of the actuators of an aircraft elevator effectivly.

## 6.2 Recommendations

Nowadays, ELSs are used in various technical fields such as robotics, aerospace, wind energy, and elevator systems. This work is limited to simulation using MATLAB/Simulink. I recommend the hardware implementation of this an Electric Load Simulator based on GWO-STSMC. In this thesis, a torque sensor is used to measure the loading torque applied to the tested system. Loading torque from the torque sensor needs to be added to a filter like a Kalman filter to improve the accuracy of this system more.

In this thesis work, the reference position command of the actuator system is used only as an input to the aerodynamic load calculator system. I recommend that, taking into account air speed, Mach number, and angle of attack for the input of the aerodynamic load calculator, in addition to the reference position command of the actuator system for future work.

## Research Fund Acknowledgment

This research thesis was funded by Adama Science and Technology University under the grant number of **ASTU/SM-R/568/22**, Adama, Ethiopia.

# REFERENCES


Akova, H. U. (2014). Design, construction and control of an electro-hydraulic load simulator for testing hydraulic drives. *Asian J. Control* , 22(9), 634-715. https://hsgm.saglik.gov.tr/depo/birimler/saglikli-beslenme-hareketli-hayat-db/Yayinlar/kitaplar/diger-kitaplar/TBSA-Beslenme-Yayini.pdf

Astrom, K. J., Wit, C. C. De, Astrom, K. J., Canudas, C., & Revisiting, D. W. (2009). Revisiting the LuGre friction model. *28*(6), 101–114

Becker, F. G., Cleary, M., (2015). Adaptive predicting control for electrical load simulator *Syria Studies*, 7(1), 37–72. https://www.researchgate.net/publication/269107473_What_is_governance/link/548173090cf22525dcb61443/download%0.

Chu, H., Zhang, M., Zhou, M., Liu, H., Zhang, B., & Zhang, Y. (2018). Friction compensation and observer-based adaptive sliding mode control of electromechanical actuator. *Advances in Mechanical Engineering*, 10(12), 1–15. https://doi.org/10.1177/1687814018813793

Copeland, B. (2008). The Design of PID Controllers using Ziegler Nichols Tuning. Retrieved, March, March, 1–4. http://educypedia.karadimov.info/library/Ziegler_Nichols.pdf

Cucuzzella, M. (n.d.). Design and Analysis of Sliding Mode Control Algorithms for Power Networks. *Research Journal of Applied Sciences, Engineering and Technology.* 204-256.

Dai, M., Qi, R., Zhao, Y., & Li, Y. (2021). PD-type iterative learning control with adaptive learning gains for high-performance load torque tracking of electric dynamic load simulator. *Electronics (Switzerland)*, *10*(7). https://doi.org/10.3390/electronics10070811

Do, N. B. (2005). Modeling of frictional contact conditions in structures.

Fu, J. (2017). Review on signal-by-wire and power-by-wire actuation for more electric aircraft. Chinese Journal of Aeronautics vol. *30*, pp. 857–870. https://doi.org/10.1016/j.cja.2017.03.013

Fu, Y., Zhou, W., Zhang, Y., Zheng, L., & Pang, Y. (2010). Robust and perfect tracking control for direct drive EMA system. *Proceedings of 2010 International Conference on Intelligent Control and Information Processing, ICICIP 2010*, PART 1, 738–743. https://doi.org/10.1109/ICICIP.2010.5564327

Gao, J., Zhou, Y., & Zhang, Y. (2021). Research on load simulator control methods for aircraft actuation system. *Proceedings - 2019 International Conference on Sensing, Diagnostics, Prognostics, and Control, SDPC 2019*, 318–322. https://doi.org/10.1109/SDPC.2019.00064

Guo, B., Wang, M. Y., & Zhang, J. (2006). A dynamic fuzzy neural networks controller for dynamic load simulator. *Proceedings of the 2006 International Conference on Machine Learning and Cybernetics*, 375–379. https://doi.org/10.1109/ICMLC.2006.259042

Haugen, F. (n.d.). zn_open_loop_method_3.pdf.

Helsinki, U. D. E. T. D. (2008). Pid controller design and tuning in networked. *Helsinki University of Technology Control Engineering*. vol. 23, pp. 45-98.

Jia, Y., & Jie, Y. (2018). Research on electric load simulator based on dual loop control. *2018 IEEE 4th Information Technology and Mechatronics Engineering Conference (ITOEC), Itoec*, 1933–1936.

Ka'ka, S., Himran, S., Renreng, I., & Sutresman, O. (2017). Pneumatic actuator as vertical dynamic load simulator on the suspension mechanism of a quarter vehicle wheels. *ARPN Journal of Engineering and Applied Sciences*, *12*(23), 6975–6980.

Kapoor, A., Simaan, N., & Kazanzides, P. (2004). A System for Speed and Torque Control of DC Motors with Application to Small Snake Robots. http://www.cs.jhu.edu/~kapoor/lopomoco/mechrob.pdf

Khan, M. K. (2003). Design and application of second order sliding mode control algorithms. *Thesis submitted for the degree of Doctor of Philosophy at the University of Leicester.*

Li, C., Pan, X., & Wang, G. (2018). Torque tracking control of electric load simulator with active motion disturbance and nonlinearity based on T-S fuzzy model. *Asian Journal of Control*, *22*(3), 1280–1294. https://doi.org/10.1002/asjc.2009

Liu, J., & Khayati, K. (2022). Adaptive Super-Twisting Sliding Mode Control for Nonlinear Dynamic Systems with Unknown Polynomial Perturbations. *Journal of Hubei University of Science and Techology*, vol.2,pp. 0–20.

Liu, X., Wu, Y., Deng, Y., & Xiao, S. (2014). A global sliding mode controller for missile electromechanical actuator servo system. *Proceedings of the Institution of Mechanical Engineers, Part G: Journal of Aerospace Engineering*, *228*(7), 1095–1104. https://doi.org/10.1177/0954410013485522

Lv, H., Wang, Z., Zhou, X., Chen, Z., & Yang, Y. (2018). Design and modeling of a test bench for dual-motor electric drive tracked vehicles based on a dynamic load emulation method. *Sensors (Switzerland)*, *18*(7). https://doi.org/10.3390/s18071993

Mancini, M. (2019). Obstacle Avoidance for Rendezvous Maneuver. *Master of Science in Aerospace Engineering Master Thesis Sliding Mode Techniques and Dynamic.*

Mirjalili, S., Mirjalili, S. M., Lewis, A., Optimizer, G. W., Mirjalili, S., Mirjalili, S. M., Lewis, A., Technology, C., & Beheshti, S. (2014). *Grey Wolf Optimizer 1 1*. *69*, 46–61.

MOHAMAD, A. A. B., & A. (2012). Simulation of auto –tuning pid controller for dc motor using ziegler-nichols method aina. *The Lancet Neurology*, *11*(9), 753. https://doi.org/10.1016/S1474-4422(12)70197-7

Nasim Ullah. (2016). Loads Simulator System for Testing and Qualification of Flight Actuators. *Intech*, 13. http://dx.doi.org/10.1016/j.colsurfa.2011.12.014

Patel, V. V. (2020). Ziegler – Nichols Tuning Method. *Control System Design Guide (Fourth Edition)*, *25*(10), 1385–1397.

Qiao, G., Liu, G., Shi, Z., Wang, Y., Ma, S., & Lim, T. C. (2018). A review of electromechanical actuators for More/All Electric aircraft systems. *Proceedings of the Institution of Mechanical Engineers, Part C: Journal of Mechanical Engineering Science*, *232*(22), 4128–4151.

Rhif, A., Kardous, Z., Ben, N., & Braiek, H. (2013). First and High Order Sliding Mode-Multimodel Stabilizing Control Synthesis using Single and Several Sliding Surfaces for Nonlinear Systems : Simulation on an Autonomous Underwater Vehicles ( AUV ). Proceeding Engineering and Technology vol.1, pp.100-110.

Rogner, I. (2017). Friction modelling for robotic applications with planar motion. *Department of*

*Electrical Engineering*.

Ruan, W., Dong, Q., Zhang, & Li, Z. (2021). Friction compensation control of electromechanical actuator based on neural network adaptive sliding mode. *Sensors*, *21*(4), 1–14. https://doi.org/10.3390/s21041508

Runyon, A. N. (2019). Observer design and active fault tolerant control for Takagi-Sugeno systems affected by sensors faults. *Academia.Edu*, 1–189.

Salloum, R., Arvan, M. R., & Moaveni, B. (2016). Identification , uncertainty modeling and robust controller design for an electromechanical actuator. *Academia.Edu vol.3*, 1–11. https://doi.org/10.1177/0954406215616141

Sekhri, E. (2017). Design of a robust controller using sliding mode technique for a linear belt-driven system. *master thesis student Supervisor*. 64.

Sensors, T. (n.d.). *Torque sensors*.

Shamisa, A., & Kiani, Z. (2018). Robust fault-tolerant controller design for aerodynamic load simulator. *Aerospace Science and Technology*, *78*(April), 332–341. https://doi.org/10.1016/j.ast.2018.04.035

Shtessel, Y., Edwards, C., Fridman, L., & Levant, A. (n.d.). Sliding Mode Control and observation. *Control Engineering (CONTRENGIN).*

Smuts, J. (2011). *Process Control for Practitioners*. 1–27.

Syaifudin. (2015). Nature Inspired Grey Wolf Optimizer Algorithm for Minimizing Operating Cost in Green Smart Home. *Ekp*, *13*(3), 1576–1580.

Tayyeb, M., Riaz, U., Amin, A. A., Saleem, O., Arslan, M., & Shahbaz, M. H. (2021). Design of highly redundant fault tolerant control for aircraft elevator system. *Journal of Applied Engineering Science*, *19*(1), 37–47. https://doi.org/10.5937/jaes0-27611

Tenali, V. S. (2007). *Simualation of Electro-Hydraulic Servo Actuator*. *769008*, 73.

Ullah, N., Khan, W., & Wang, S. (2014). High performance direct torque control of electrical aerodynamics load simulator using fractional calculus. *Acta Polytechnica Hungarica*, *11*(10), 59–78.

Verma, N. (2021). *H-MPGWO :* A Hierarchical Multi-Population Grey Wolf Optimization Framework.

Wang, L., Wang, M., Guo, B., Wang, Z., Wang, D., & Li, Y. (2016). Analysis and Design of a Speed Controller for Electric Load Simulators. *63*(12), 7413–7422.

Wang, L., Wang, M., Guo, B., Wang, Z., Wang, D., & Li, Y. (2018). A Loading Control Strategy for Electric Load Simulators Based on Proportional Resonant Control. *IEEE Transactions on Industrial Electronics*, *65*(6), 4608–4618. https://doi.org/10.1109/TIE.2017.2756585

Wang, X., Wang, S., & Yao, B. (2013). Adaptive robust torque control of electric load simulator with strong position coupling disturbance. *International Journal of Control, Automation and Systems*, *11*(2), 325–332. https://doi.org/10.1007/s12555-011-0181-8

Zhang, J., Fan, Y., Cao, D., Lu, P., & Zhang, J. (2021). Backstepping sliding mode control of electric linear load simulator. *Journal of Physics: Conference Series*, *1754*(1). https://doi.org/10.1088/1742-6596/1754/1/012111

# APPENDICES

## Appendixes A

### Simulink block diagram

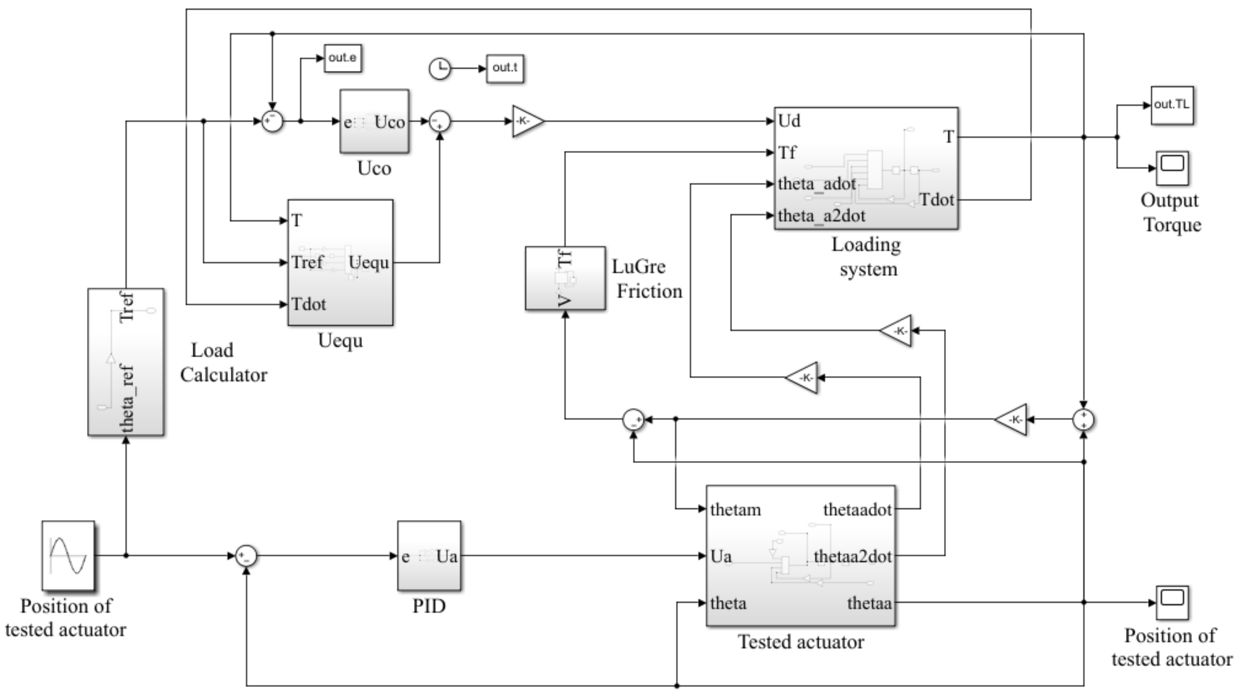


Figure A. 1:- Simulink Block for GWO-STSMC

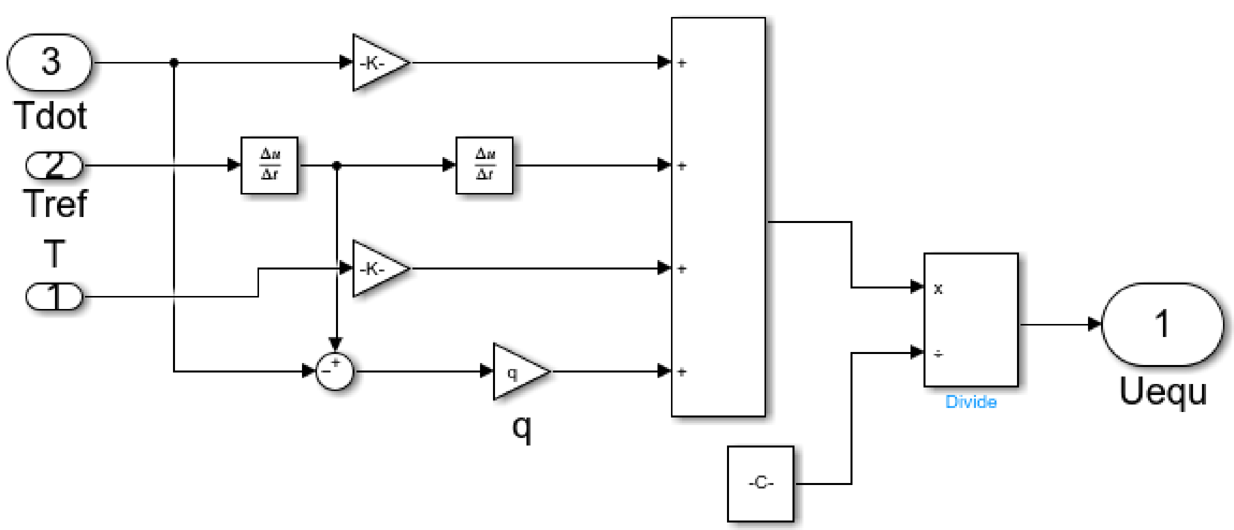


Figure A. 2:- Simulink Block for equivalent control ($U_{equ}$)

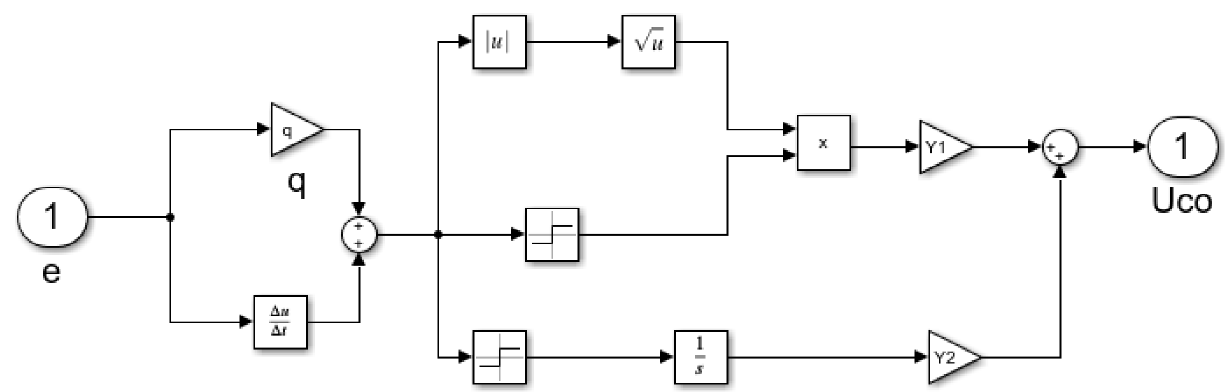


Figure A. 3:- Simulink Block for discrete control ($U_{co}$)

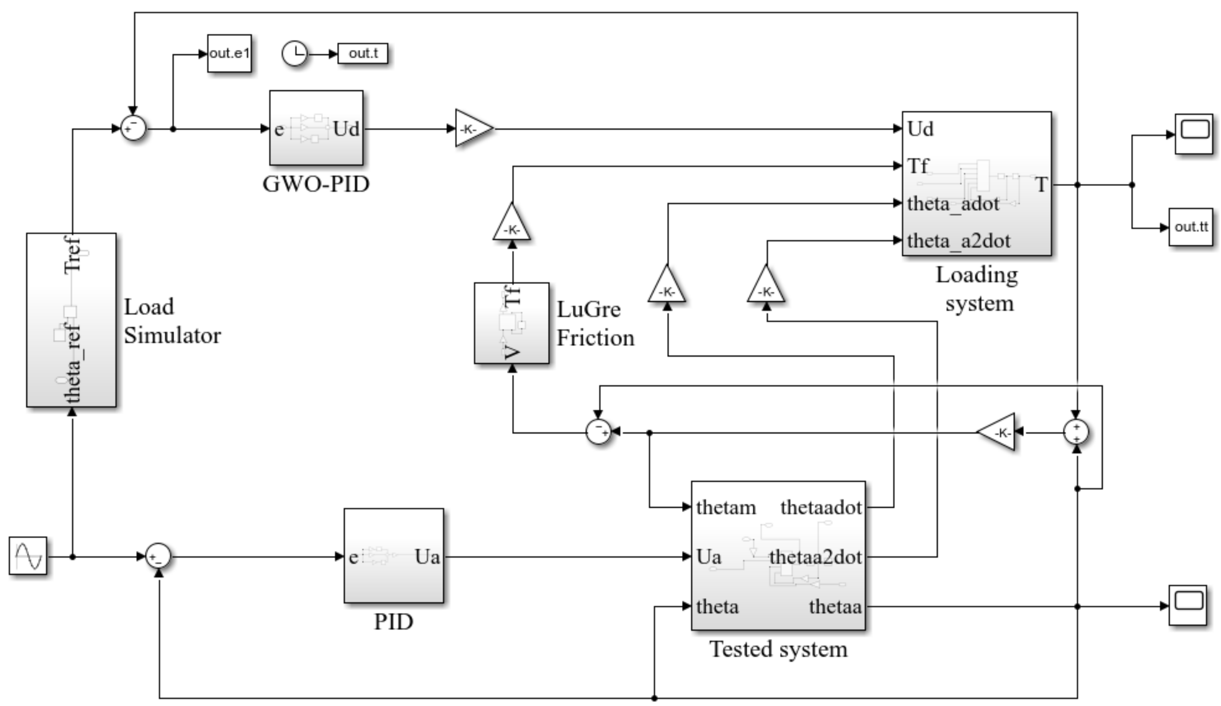


Figure A. 4:- Simulink Block for GWO-PID.

# Appendixes B

**Test algorithm to determine boundary of STSMC and PID parameters**

```
function test
warning('off')
Kp=0.0001;Ki=0.0001;Kd=0.0001;
x=[q Y1 Y2];
obj= object(x)
%%
% Measures a performance index from the simulink model
function obj = object(x)
simulink_model = 'sine_STSMC_GWO';
load_system(simulink_model);
gains= getparam(simulink_model,'modelworkspace');
gains.assignin('q', x(1));
gains.assignin('Y1', x(2));
gains.assignin('Y2', x(3));
%
simOut = sim(simulink_model,'SaveOutput','on');
 t = simOut.find('t');
e1 = simOut.find('e');
n=size(e1);
obj= 0;
for i = 2:n
   stepsize = t(i)-t(i-1);
   obj = obj+0.5*(ea(i-1)+ea(i))*stepsize;
```

**Grey wolf optimization algorithm for STSMC**

```
% Tune the gains of the STSMC controller using a GWO
fobj =  @object; % cost function
dim  = 3; % number of parameter
Max_iteration   = 20;
SearchAgents_no = 20;
lb = [0.0001 0.0001 0.0001];
ub = [10 15 30];
```

```
[Best_score,Best_pos,GWO_cg_curve]=GWO(SearchAgents_no,Max_iteration,lb,ub,dim,fobj);
%%  incase of plot
semilogy(GWO_cg_curve,'Color','r');
xlabel('Iteration');
ylabel('fitness value');
axis tight;
grid on;
box on;legend('GWO');
title(['best: ', num2str(Best_score)]);
display(['The best value: ', num2str(Best_score)]);
% Grey Wolf Optimizer
function
[Alpha_score,Alpha_pos,Convergence_curve]=GWO(SearchAgents_no,Max_iter,lb,ub,dim,fobj
 % initialize alpha, beta, and delta_pos
Alpha_pos=zeros(1,dim);
Alpha_score=inf; %change this to -inf for maximization problems
Beta_pos=zeros(1,dim);
Beta_score=inf; %change this to -inf for maximization problems
Delta_pos=zeros(1,dim);
Delta_score=inf; %change this to -inf for maximization problems
 %Initialize the positions of search agents
Positions=initialization(SearchAgents_no,dim,ub,lb);
 Convergence_curve=zeros(1,Max_iter);
 l=0;% Loop counter
 % Main loop
while l<Max_iter
    for i=1:size(Positions,1)
        Flag4ub=Positions(i,:)>ub;
        Flag4lb=Positions(i,:)<lb;
       Positions(i,:)=(Positions(i,:).*(~(Flag4ub+Flag4lb)))+ub.*Flag4ub+lb.*Flag4lb;
       % Calculate objective function for each search agent
```

```
  fitness=fobj(Positions(i,:));
 % Update Alpha, Beta, and Delta
  if fitness<Alpha_score
     Alpha_score=fitness; % Update alpha
     Alpha_pos=Positions(i,:);
  end
   if fitness>Alpha_score && fitness<Beta_score
     Beta_score=fitness; % Update beta
     Beta_pos=Positions(i,:);
  end
  if fitness>Alpha_score && fitness>Beta_score && fitness<Delta_score
     Delta_score=fitness; % Update delta
     Delta_pos=Positions(i,:);
  end
end
a=2-l*((2)/Max_iter); % a decreases linearly fron 2 to 0
% Update the Position of search agents including omegas
for i=1:size(Positions,1)
  for j=1:size(Positions,2)
     r1=rand(); % r1 is a random number in [0,1]
     r2=rand(); % r2 is a random number in [0,1]
     A1=2*a*r1-a; % Equation (3.3)
     C1=2*r2; % Equation (3.4)
     D_alpha=abs(C1*Alpha_pos(j)-Positions(i,j)); % Equation (3.5)
     X1=Alpha_pos(j)-A1*D_alpha; % Equation (3.6)-part 1
     r1=rand();
     r2=rand();
     A2=2*a*r1-a; % Equation (3.3)
     C2=2*r2; % Equation (3.4)
     beta=abs(C2*Beta_pos(j)-Positions(i,j)); % Equation (3.5)-part 2
     X2=Beta_pos(j)-A2*D_beta; % Equation (3.6)-part 2
```

```
            r1=rand();
            r2=rand();
            A3=2*a*r1-a; % Equation (3.3)
            C3=2*r2; % Equation (3.4)
            D_delta=abs(C3*Delta_pos(j)-Positions(i,j)); % Equation (3.5)
            X3=Delta_pos(j)-A3*D_delta; % Equation (3.5)-part 3
            Positions(i,j)=(X1+X2+X3)/3;% Equation (3.7)
            end
    end
    l=l+1;
    Convergence_curve(l)=Alpha_score;
end
function obj = object(x)
simulink_model = 'sine_STSMC_GWO';
load_system(simulink_model);
gains= getparam(simulink_model,'modelworkspace');
gains.assignin('q', x(1));
gains.assignin('Y1', x(2));
gains.assignin('Y2', x(3));
%
simOut = sim(simulink_model,'SaveOutput','on');
 t = simOut.find('t');
e1 = simOut.find('e');
n=size(e1);
obj= 0;
for i = 2:n
    stepsize = t(i)-t(i-1);
    obj = obj+0.5*(ea(i-1)+ea(i))*stepsize;
end
end
```

**Grey wolf optimization algorithm for PID**

```
fobj =  @object; % cost function
dim  = 3; % number of parameter
Max_iteration   = 20;
SearchAgents_no = 20;
lb = [0.0001 0.0001 0.0001];
ub = [25 15 10];
[Best_score,Best_pos,GWO_cg_curve]=GWO(SearchAgents_no,Max_iteration,lb,ub,dim,fobj);
%%  incase of plot
semilogy(GWO_cg_curve,'Color','r');
xlabel('Iteration');
ylabel('fitness value');
axis tight;
grid on;
box on;legend('GWO');
title(['best: ', num2str(Best_score)]);
display(['The best value: ', num2str(Best_score)]);
% Grey Wolf Optimizer
function
[Alpha_score,Alpha_pos,Convergence_curve]=GWO(SearchAgents_no,Max_iter,lb,ub,dim,fobj
 % initialize alpha, beta, and delta_pos
Alpha_pos=zeros(1,dim);
Alpha_score=inf; %change this to -inf for maximization problems
Beta_pos=zeros(1,dim);
Beta_score=inf; %change this to -inf for maximization problems
Delta_pos=zeros(1,dim);
Delta_score=inf; %change this to -inf for maximization problems
 %Initialize the positions of search agents
Positions=initialization(SearchAgents_no,dim,ub,lb);
 Convergence_curve=zeros(1,Max_iter);
 l=0;% Loop counter
```

```
 % Main loop
while l<Max_iter
    for i=1:size(Positions,1)
        Flag4ub=Positions(i,:)>ub;
        Flag4lb=Positions(i,:)<lb;
       Positions(i,:)=(Positions(i,:).*(~(Flag4ub+Flag4lb)))+ub.*Flag4ub+lb.*Flag4lb;
       % Calculate objective function for each search agent
        fitness=fobj(Positions(i,:));
       % Update Alpha, Beta, and Delta
        if fitness<Alpha_score
            Alpha_score=fitness; % Update alpha
            Alpha_pos=Positions(i,:);
        end
          if fitness>Alpha_score && fitness<Beta_score
            Beta_score=fitness; % Update beta
            Beta_pos=Positions(i,:);
        end
        if fitness>Alpha_score && fitness>Beta_score && fitness<Delta_score
            Delta_score=fitness; % Update delta
            Delta_pos=Positions(i,:);
        end
    end
    a=2-l*((2)/Max_iter); % a decreases linearly fron 2 to 0
    % Update the Position of search agents including omegas
    for i=1:size(Positions,1)
        for j=1:size(Positions,2)
            r1=rand(); % r1 is a random number in [0,1]
            r2=rand(); % r2 is a random number in [0,1]
            A1=2*a*r1-a; % Equation (3.3)
            C1=2*r2; % Equation (3.4)
            D_alpha=abs(C1*Alpha_pos(j)-Positions(i,j)); % Equation (3.5)
```

```
            X1=Alpha_pos(j)-A1*D_alpha; % Equation (3.6)-part 1
            r1=rand();
            r2=rand();
            A2=2*a*r1-a; % Equation (3.3)
            C2=2*r2; % Equation (3.4)
            beta=abs(C2*Beta_pos(j)-Positions(i,j)); % Equation (3.5)-part 2
            X2=Beta_pos(j)-A2*D_beta; % Equation (3.6)-part 2
            r1=rand();
            r2=rand();
            A3=2*a*r1-a; % Equation (3.3)
            C3=2*r2; % Equation (3.4)
            D_delta=abs(C3*Delta_pos(j)-Positions(i,j)); % Equation (3.5)
            X3=Delta_pos(j)-A3*D_delta; % Equation (3.5)-part 3
            Positions(i,j)=(X1+X2+X3)/3;% Equation (3.7)
            end
    end
    i=i+1;
    Convergence_curve(l)=Alpha_score;
end
function obj = object(x)
simulink_model = 'sine_PID_GWO';
load_system(simulink_model);
gains= getparam(simulink_model,'modelworkspace');
gains.assignin('Kp', x(1));
gains.assignin('Ki', x(2));
gains.assignin('Kd', x(3));
%
simOut = sim(simulink_model,'SaveOutput','on');
 t = simOut.find('t');
e1 = simOut.find('e1');
n=size(e1);
```

```
obj= 0;
for i = 2:n
    stepsize = t(i)-t(i-1);
    obj = obj+0.5*(ea(i-1)+ea(i))*stepsize;
end
end
```